

Variational Distillation for Multi-View Learning

Xudong Tian, Zhizhong Zhang, Cong Wang, Wensheng Zhang, Yanyun Qu, Lizhuang Ma,
Zongze Wu, Yuan Xie, *Member, IEEE*, Dacheng Tao, *Fellow, IEEE*

Abstract—Information Bottleneck (IB) based multi-view learning provides an information theoretic principle for seeking shared information contained in heterogeneous data descriptions. However, its great success is generally attributed to estimate the multivariate mutual information which is intractable when the network becomes complicated. Moreover, the representation learning tradeoff, *i.e.*, prediction-compression and sufficiency-consistency tradeoff, makes the IB hard to satisfy both requirements simultaneously. In this paper, we design several variational information bottlenecks to exploit two key characteristics (*i.e.*, sufficiency and consistency) for multi-view representation learning. Specifically, we propose a Multi-View Variational Distillation (MV²D) strategy to provide a scalable, flexible and analytical solution to fitting MI by giving arbitrary input of viewpoints but without explicitly estimating it. Under rigorously theoretical guarantee, our approach enables IB to grasp the intrinsic correlation between observations and semantic labels, producing predictive and compact representations naturally. Also, our information-theoretic constraint can effectively neutralize the sensitivity to heterogeneous data by eliminating both task-irrelevant and view-specific information, preventing both tradeoffs in multiple view cases. To verify our theoretically grounded strategies, we apply our approaches to various benchmarks under three different applications. Extensive experiments to quantitatively and qualitatively demonstrate the effectiveness of our approach against state-of-the-art methods.

Index Terms—multi-view learning, Information bottleneck, mutual information, variational inference, knowledge distillation.



1 INTRODUCTION

As more and more real-world data are collected from diverse sources or obtained from different feature extractors, multi-view representation learning has gained increasing attention due to its strong predictive power. For example, in auto-driving scene, there usually exist camera sensors that assist LiDAR data to perceive the complex 3D visual world, and therefore it enables us to take advantages of depth, texture and color information provided by multiple sensors to improve the predictive performance. From this perspective, multi-view learning aims to integrate various features (*i.e.*, heterogeneous data or visual descriptors) of the same object to promote the performance of existing machine learning system.

To effectively explore multi-view data, many efforts have been devoted to learning a consistent representation for discriminative information mining, such as Canonical Correlation Analysis (CCA) [1], [2] or feature alignment [3],

both of which primarily maximize the similarity between representations from different viewpoints, and are more prone to introduce non-predictive redundancy and even cause considerable loss of predictive information.

Among various solutions, information bottleneck (IB) provides an information-theoretic principle [4] for multi-view learning, which has been successfully applied to a wide range of applications. [5], [6], [7]. The central role of IB is to fit mutual information (MI) to maximize the correlation between representation and predictive information, while avoiding encoding task-irrelevant information. However, practical use of IB remains a persistent challenge due to the notorious difficulty of estimating mutual information. To deal with this, a common practice is to adopt the trainable parametric neural estimators [8], [5], [9] involving reparameterization trick, sampling, estimation of posterior distribution [10], which, unfortunately, have relatively poor scalability in practice, and even become intractable when the network is complicated.

Another principal drawback of the information bottleneck is that, its optimization objective is essentially a trade-off between having a concise representation and achieving good predictive power, which makes it impossible to realize both high compression and accurate prediction [4], [11], [12]. Worse still, when dealing with heterogeneous data descriptions [5], [6], [7], it has to struggle with multivariate mutual information to strike a balance between complementarity and consistency. Therefore, we raise a critical question: How to effectively explore the useful predictive information to learn a meaningful representation from multi-view data?

In this paper, we propose a new multi-view information bottleneck strategy, named as Multi-View Variational Distillation (MV²D), for generalized multi-view representation learning. In this framework, we use variational inference to reconstruct the objective of IB and provide an analytical

- X. Tian, Z. Zhang, and Y. Xie are with School of Computer Science and Technology, East China Normal University, Shanghai, 200062, China; E-mail: {52215901004, zzzhang, yxie}@cs.ecnu.edu.cn
- C. Wang is with the Distributed and Parallel Software Laboratory, 2012 Labs, Huawei Technologies, Hangzhou, China; E-mail: wangcong64@huawei.com
- W. Zhang is with Institute of Automation, Chinese Academy of Sciences, Beijing, 100190, China; E-mail: wensheng.zhang@ia.ac.cn
- Y. Qu is with School of Information Science and Technology, Xiamen University, Fujian, 361005, China; E-mail: yyqu@xmu.edu.cn
- L. Ma is with School of Computer Science and Technology, East China Normal University, Shanghai, and also with the School of Electronic Information and Electrical Engineering, Shanghai Jiao Tong University, China; E-mail: lzma@cs.ecnu.edu.cn
- Z. Wu is with College of Mechatronics and Control Engineering, Shenzhen University, Shenzhen, China; E-mail: zzwu@szu.edu.cn
- D. Tao is with JD Explorer Academy, China and the University of Sydney, Australia; E-mail: dacheng.tao@gmail.com

solution to MV²D, which drives the network towards learning concise yet predictive representations under a consistent training goal, by **fitting mutual information without explicitly estimating it**. Specifically, MV²D consists of two components (*i.e.*, sufficiency and consistency), where the first one enables us to preserve sufficient task-relevant information, while simultaneously discarding task-irrelevant distractors; and the second one neutralizes the sensitivity to multi-view data by refining the consistent information.

MV²D is applicable to arbitrary input of viewpoints and can identify the prioritization for each representation by automatically exploring the useful consistent multi-view information. The resulting representations are then improved with enhanced generalization ability and robustness to the heterogeneous gap among different viewpoints. In addition, we show existing cutting-edge variational information bottleneck like Variational Self-Distillation (VSD), Variational Cross Distillation (VCD), Variational Mutual Distillation (VMD) [13] are the special cases of our MV²D framework. MV²D and all its variants do not require any strong assumptions or mutual information estimators, and can concurrently attain two key characteristics of representation learning (*i.e.*, sufficiency and consistency) under rigorously theoretical guarantee.

To verify our theoretically grounded strategies in single-view, cross-view and multi-view cases, we apply our approaches to the tasks of: (i) Cross-modal person re-identification¹; (ii) Multi-view classification; (iii) LiDAR-RGB semantic segmentation. Extensive experiments conducted on the widely adopted benchmark datasets demonstrate the effectiveness, robustness and superior performance of our approaches against state-of-the-arts methods. Our main contributions are summarized as follows:

- We design a new information bottleneck strategy for multi-view representation learning, with arbitrary input of views, named as Multi-View Variational Distillation (MV²D), which is able to prevent both the prediction-compression and sufficiency-consistency trade-off, leading to a predictive and consistent representation.
- Under strictly mathematical proofs, we introduce a generalized analytical solution to maximizing consistent information among multiple heterogeneous data observations, which significantly improves the robustness to view-changes by accurately eliminating both the view-specific and non-predictive details.
- We show the proposed variational distillation framework could be flexibly applied to diverse multi-view tasks. The experiments on Cross-modal person re-identification; Multi-view classification and LiDAR-RGB semantic segmentation demonstrate the effectiveness of our approach.

2 RELATED WORK

2.1 Information Bottleneck

The seminal work of Information Bottleneck is from [4], [14], which introduces the general idea of using the

information theoretic objective to train a deep model. But, unfortunately, they did not include any experimental results, since the optimization for IB relied on the iterative Blahut Arimoto algorithm, which is infeasible over high-dimensional variables, *e.g.*, deep neural networks (DNNs) [11]. On this basis, a series of explorations from theoretic study to practical use of IB principle have been witnessed.

Theoretic Study of IB. By using the variational inference and re-parameterization tricks, VIB [11] constructs a lower bound on IB objective (Eq. (3)), and enables the DNNs to handle the high-dimensional and continuous data under the guidance of IB. It avoids the restrictions that data must follow discrete or Gaussian distribution. Moreover, with the introduction of dual distortion [15], dualIB framework is presented in [12], which shifts the research attention from training to prediction, leading to the better stability compared with the classic IB structure. However, these methods still suffer from IB’s disadvantage (*i.e.*, the trade-off between prediction and compression) and consequently have unsatisfactory applicability for real world problems.

Practical Applications of IB. Typically, [16] applies Eq. (3) to the generative adversarial networks (GANs), with small modifications for a more robust generation process. [17] alleviates the overfitting of large-scale pretrained language models in low-resource scenarios by directly introducing Eq. (3). Other applications involving IB include decision-making system [18], speech processing [19], ensemble learning [20], neuroscience [21] and deep neural networks understanding [22]. However, they either heavily rely on the mutual information estimator, or reformulate the IB objective based on strong assumptions, resulting in inferior practicality.

In contrast to all of the above, our work is the first to provide an analytical solution to fitting the mutual information without estimating it. The proposed VSD can better preserve task-relevant information, while simultaneously getting rid of redundant nuisances.

2.2 Representation Learning

The performance of machine learning methods is heavily dependent on the learned representations, which may entangle or hide different explanatory factors behind the data. Hence, a great deal of researches is devoted to designing data processing pipelines or transformations to attain representations that can support effective machine learning. Specifically, early works prefer feature engineering (we refer readers to [23] for comprehensive studies) to take advantage of human ingenuity and prior knowledge. After that, numerous deep models adopt reconstruction-based [2] representation, which enforces similarity constraint between the input and reconstructed output; or contrastive methods [24], which learn representations by maximizing similarity between augmentations of the same data point and minimizing similarity between different data points.

Unfortunately, feature engineering is labor-intensive, and shows inferiority to extract discriminative information in complex circumstances [23]. Moreover, reconstruction-based and contrastive methods highly rely on similarity maximization, which are more prone to overfitting or obtain a trivial solution when encountering small scale datasets. On

1. We do not explicitly distinguish multi-view and multi-modal throughout this paper.

TABLE 1: Basic notations and their descriptions.

Notation	Meaning
x, y v, z	object, and the corresponding ground-truth label observation, representation of x
$\{x_1, \dots, x_n\}$ $\{v_1, \dots, v_n\}$ $\{z_1, \dots, z_n\}$ $z_{\{1, \dots, n\}/i}$	multiple views of the same object x observations collected from different viewpoints multi-view representations, denoted as $z_{\{1, \dots, n\}}$ the entire $\{z_1, \dots, z_n\}$ but excluding z_i
$I(v; z)$ $I(v; z y)$ $I_{z_1 y z_2 z_3}$ $I_{y z_1 z_2 z_3}$ $I_{y z_1 z_2 z_3}$ $I_{y z_1 z_2 z_3}$	mutual information, denoted as MI for simplicity conditional MI, abbreviated as $I_{vz y}$ in diagrams information unique to z_1 , i.e., $H(z_1 y, z_2, z_3)$ conditional MI between y and z_1 , i.e., $I(y; z_1 z_2, z_3)$ MI among y, z_1 and z_2 , i.e., $I(y; z_1; z_2 z_3)$ information shared by y, z_1, z_2, z_3 , i.e., $I(y; z_1; z_2; z_3)$
E_θ, E_ϕ $H(\cdot), H(\cdot \cdot)$ $\mathbb{P}_v, \mathbb{P}_z$ $\mathbb{P}_{z_{\{1, \dots, n\}/i}}$	the encoder and information bottleneck Shannon entropy, conditional entropy predictions conditioned on v and z prediction conditioned on $z_{\{1, \dots, n\}/i}$

the contrary, our approach enables the model to accurately preserve predictive information *w.r.t.* the given task while discarding those superfluous under the information theoretic constraint towards generalized representation learning. More importantly, our approach is quite efficient since it does not require large-scale training data or batch size.

2.3 Multi-Modal/View Representation Learning

Multi-modal representation learning aims to build models that can process and relate information from multiple modalities, and its main difficulty is to explicitly measure the content similarity between the heterogeneous samples. Classical and deep multi-view representation learning methods can be roughly divided into joint representation [25], [1], alignment representation [3], [26], as well as shared and specific representation [27], [28]. The key idea of these methods is to establish a common representation space by exploring the semantic relationship among multi-view data. Please refer to [29], [30] for a comprehensive review.

Recently, another line of works (*e.g.*, MIB [5] and MVIB [6]) extend IB principle to the multi-view representation learning, which achieves promising results. For example, MIB integrates the heterogeneous representations by introducing a variational bound of Eq. (3). However, it still requires explicit estimation to the mutual information, and is applicable when only two views are entailed. Consequently, it shows weak scalability for complex cases, and fails to learn a generalized representation for arbitrary input of viewpoints. By comparison, the proposed MV²D avoids both the prediction-compression trade-off and sufficiency-consistency trade-off, enabling us to learn a predictive yet compact representation. The empirical study also demonstrates that our method can effectively eradicate both the non-predictive and view-specific information and thus significantly improve the robustness and generalization ability.

2.4 Knowledge Distillation

Knowledge distillation (KD) is a representative technique utilized for model compression and acceleration, which typically intends to learn a small student model from a large-scale teacher by minimizing a KL-divergence loss between their predictions. In addition to the student-teacher paradigm, recent developments have been extended

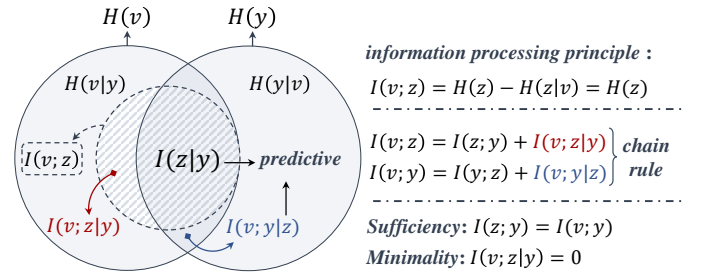


Figure 1: Venn diagram visualization of entropies and mutual information for three variables v, z and y .

to assistant-learning [31], mutual-learning [32] and self-learning [33] (please refer to [34] for more related works). Despite the wide use of KD, fundamental analysis of what information should be distilled is still lacking in the literature, remaining the mechanism of KD still unclear.

3 PRELIMINARY

In this section, we first provide a brief review of the IB principle [4] in the context of supervised learning. Then we introduce several variations of mutual information encompassed in our method. We summarize the basic notations and their descriptions in Tab. 1.

3.1 Information Bottleneck Principle

Given data observations V and labels Y , the goal of representation learning is to obtain an encoding Z which is maximally informative *w.r.t.* Y (*i.e.*, **sufficiency** in Fig. 1), and without any additional information about V (*i.e.*, **minimality** in Fig. 1), measured by mutual information, *i.e.*,

$$I(Z; Y) = \int p(z, y) \log \frac{p(z, y)}{p(z)p(y)} dz dy. \quad (1)$$

Based on the information processing principle, we illustrate the definitions of sufficiency and minimality in Fig. 1, where the areas of the three circles represent $H(v)$, $H(y)$ and $H(z)$. To encourage the encoding process to focus on the label information, IB was proposed to enforce an upper bound I_c to the information flow from the observations V to the encoding Z , by maximizing the following objective:

$$\max I(Z; Y) \text{ s.t. } I(Z; V) \leq I_c. \quad (2)$$

Eq. (2) implies that a compressed representation can improve the generalization ability by ignoring irrelevant distractors in the original input. By using a Lagrangian objective, IB allows the encoding Z to be maximally expressive about Y while being maximally compressive about X by:

$$\mathcal{L}_{IB} = I(Z; V) - \beta I(Z; Y), \quad (3)$$

where β is the Lagrange multiplier. However, it has been shown that it is impossible to achieve both objectives in Eq. (3) practically [5], [11] due to the trade-off optimization between high compression and high mutual information.

More significantly, estimating mutual information in high dimension imposes additional difficulties [10], [9] for optimizing IB. As a consequence, it inevitably introduces irrelevant distractors and discards some predictive cues in

the encoding process. In Sec. 4, we show how we design a new strategy to deal with these issues, and extend it to cross-modality learning, and even generalize to multi-view representation learning.

3.2 The Chain Rule of Mutual Information

The chain rule [35], [11], [5] can be utilized to subdivide the mutual information into multiple terms (e.g., $I(v; z)$ and $I(v; y)$ in Fig. 1), which are defined and visualized in Fig. 1 and Fig. 2. On this basis, numerous variants measuring statistical dependencies among different variables can be expressed, such as conditional mutual information [5], [35], interaction information [36] and total correlation [37].

However, in practice, estimating the mutual information with even the simplest form (e.g., $I(v; z)$) in high dimension can be particularly challenging, let along other sophisticated variations. Thus, to deal this such issue and promote applicability of the IB principle, we next present an analytical solution to fitting the mutual information without explicitly estimating it in both single-view and multi-view cases.

4 METHOD

Let $v \in V$ be an observation of input data $x \in X$ extracted from an encoder $E(v|x)$. The challenge of optimizing an information bottleneck can be formulated as finding an extra encoding $E(z|v)$ that preserves all label information contained in v , while simultaneously discarding task-irrelevant distractors. To this end, we show the key roles of two characteristics of z , (i.e., **sufficiency** and **consistency**) based on the information theory, and design a multi-view variational information bottlenecks to keep both characteristics.

4.1 Generalized Variational Distillation for Multi-View Representation Learning

Considering $\{v_1, v_2, \dots, v_n\}$ are n observations of x that are collected from different viewpoints. An information bottleneck is used to produce representations $\{z_1, z_2, \dots, z_n\}$ for keeping all predictive information *w.r.t* label y while avoiding encoding task-irrelevant information. From this perspective, given a specific view i , the sufficiency of z_i for y could be defined as:

$$I(z_i; y) = I(v_i; y), \quad (4)$$

where v_i is the corresponding observation containing all label information. Previous work [13] has shown that finding sufficiency representation *i.e.*, Eq. 4, could be simplified to minimize the following objective:

$$\min I(v_i; y) - I(z_i; y). \quad (5)$$

This problem can be solved easily by the following theorem:

Theorem 1. *Minimizing Eq. (5) is equivalent to minimizing the subtraction of conditional entropy $H(y|z_i)$ and $H(y|v_i)$. That is:*

$$\min I(v_i; y) - I(z_i; y) \iff \min H(y|z_i) - H(y|v_i),$$

where $H(y|z_i) := - \int p(z_i) dz_i \int p(y|z_i) \log p(y|z_i) dy$.

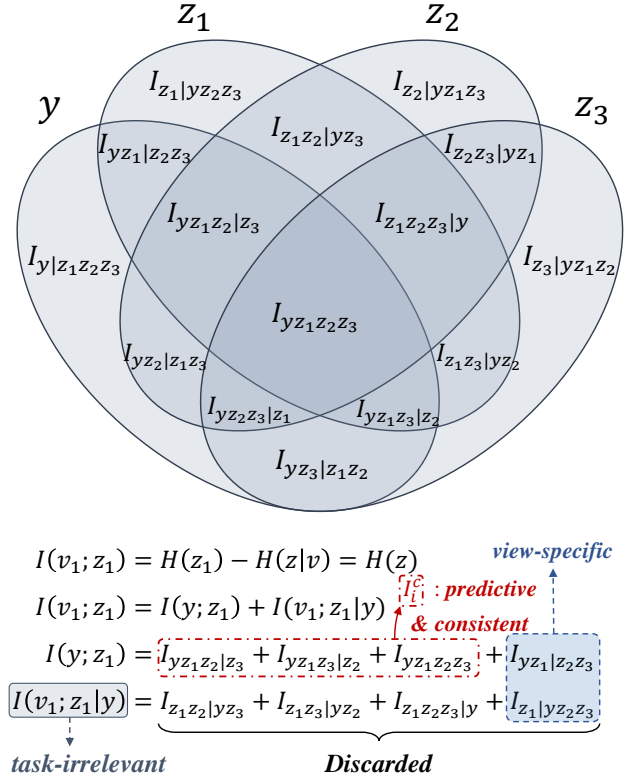


Figure 2: Venn diagram utilized to illustrate the mutual information among the target y and z_1 , z_2 and z_3 . The areas of four ellipses denote the total information of each variable. Shaded areas denote the information shared by at least two variables. Some other information measures (e.g., prediction and view-consistency) are indicated in the legend.

More specifically, given a sufficient observation v_i for y , we have the following Corollary:

Corollary 1. *If the KL-divergence between the predicted distributions of a sufficient observation v_i and the representation z_i equals to 0, then z_i is sufficient for y as well i.e.,*

$$D_{KL}[\mathbb{P}_{v_i} || \mathbb{P}_{z_i}] = 0 \implies H(y|z_i) - H(y|v_i) = 0,$$

where $\mathbb{P}_z = p(y|z_i)$, $\mathbb{P}_v = p(y|v_i)$ represent the predicted distributions, and D_{KL} denotes the KL-divergence.

The above theories reformulate the optimization objective of information bottleneck, which provides an analytical solution to achieving sufficiency for $\{z_1, z_2, \dots, z_n\}$ *w.r.t* the target y , separately. However, sufficiency is hard to attain because each representation can only partly describe the object in multi-view learning. Therefore, we introduce another strategy to promote consistency among the representations from different views.

In common practice [29], [30], consistent information is simply defined as the consensus shared by different viewpoints, which, in practice, is usually indiscriminately required to learn. However, as illustrated in Fig. 2, consistent information is essentially composed of a series of terms when multiple viewpoints are involved. Thus there is a lack of guidance to seek the useful predictive information

(e.g., terms marked with red rectangle in Fig. 2 for z_1 , vice versa for z_2 and z_2) from multi-view data. In contrast to the conventional methods, our approach highlights the prioritization for different compositions.

Though information shared by all views usually leads to better generalization (e.g., $I_{y z_1 z_2 z_3}$ in Fig. 2), it may not guarantee to be sufficient for the given task. In other words, representations learned by discarding all the information around the central area of Fig. 2 (i.e., $I_{y z_1 z_2 z_3}$) can hardly ensure predictive power for the downstream task i.e., label y . Therefore, task-relevant information should be first preserved and then assigned with different weights according to the robustness to heterogeneous gaps among different views. For example, both $I_{y z_1 z_2 | z_3}$ and $I_{y z_1 z_2 z_3}$ in Fig. 2 are supposed to be kept, and the later one should be given with larger weight since it is less sensitive to view-changes.

In the view of above, we define view-consistency to the generalized multi-view learning to clearly specify our goal. Formally, we have:

Definition 2. Consistency: For any $z_i \in \{z_1, z_2, \dots, z_n\}$, it is view-consistent iff $I(v_i; z_i | y) + I(y; z_i | z_{\{1, \dots, n\}/i}) = 0$.

In particular, $I(v_i; z_i | y)$ denotes that the information contained in z_i is unique to v_i but is not predictive w.r.t. y , i.e., superfluous information. $z_{\{1, \dots, n\}/i}$ represents the entire $\{z_1, z_2, \dots, z_n\}$ but excluding z_i , thus $I(y; z_i | z_{\{1, \dots, n\}/i})$ is the information contained in z_i but inaccessible to all other representations, i.e., view-specific information. Intuitively, consistency requires elimination of both the task-irrelevant and view-specific distractors. To that end, we first factorize $I(v_i; z_i)$ using the chain rule [5]:

$$I(v_i; z_i) = \underbrace{I(y; z_i)}_{\text{predictive}} + \underbrace{I(v_i; z_i | y)}_{\text{superfluous}}. \quad (6)$$

Notice $I(y; z_i)$ is composed of multiple terms when two or more views are involved (e.g., refer to the composition of $I(y; z_1)$ in Fig. 2). Thus, following the consistent principle in the multi-view learning, we further divide $I(y; z_i)$ as:

$$I(y; z_i) = I(y; z_i | z_{\{1, \dots, n\}/i}) + I_i^c, \quad (7)$$

where we utilize I_i^c to uniformly represent view-consistent information encoded within each z_i . For example, view-consistent information of I_1^c w.r.t z_1 in Fig. 2 is composed of $I_{y z_1 z_2 | z_3}$, $I_{y z_1 z_3 | z_2}$ and $I_{y z_1 z_2 z_3}$. This indicates I_i^c essentially includes the predictive cues shared by both z_i and all possible permutations of $\{z_1, z_2, \dots, z_n\}/z_i$.

Based on the above analysis, an initial solution can be formulated by:

$$\min \sum_{i \in n} \underbrace{-I_i^c}_{\text{consistent}} + \underbrace{I(v_i; z_i | y)}_{\text{superfluous}} + \underbrace{I(y; z_i | z_{\{1, \dots, n\}/i})}_{\text{view-specific}}, \quad (8)$$

which intuitively aims to eliminate both the task-irrelevant nuisances and view-specific information. Obviously, the min-max game of Eq. (8) is intractable to conduct. Thus, we present the following theory to equivalently reformulate our objective:

Theorem 3. Given representations $\{z_1, \dots, z_n\}$ for n different

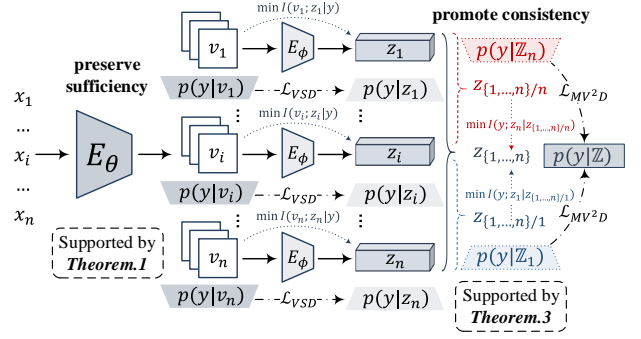


Figure 3: Illustration of the MV²D framework, where \mathbb{Z} refers to the whole $\{z_1, \dots, z_n\}$, while the subscription in \mathbb{Z}_i denotes the index of the excluded variable (e.g., $\mathbb{Z}_1, \mathbb{Z}_n$ exclude the first and the n -th representations, respectively).

views, consistency can be promoted without violating the sufficiency constraint by:

$$\min \sum_{i \in n} D_{KL}[\mathbb{P}_{v_i} || \mathbb{P}_{z_i}] + D_{KL}[\mathbb{P}_{z_{\{1, \dots, n\}}} || \mathbb{P}_{z_{\{1, \dots, n\}/i}}],$$

where $\mathbb{P}_{z_{\{1, \dots, n\}}} = p(y | z_{\{1, \dots, n\}})$, $\mathbb{P}_{z_{\{1, \dots, n\}/i}} = p(y | z_{\{1, \dots, n\}/i})$, and $\mathbb{P}_{v_i} = p(y | v_i)$ and $\mathbb{P}_{z_i} = p(y | z_i)$, all of them are essentially predicted distributions.

Detailed proof and formal assertions can be found in the Appendix. Hence, the refined training objective can be formed as:

$$\begin{aligned} \mathcal{L}_{MV^2D} = & \min_{\theta, \phi} \sum_{i \in n} \mathbb{E}_{v_i \sim E_{\theta}(v_i | x)} \mathbb{E}_{z_i \sim E_{\phi}(z_i | v_i)} [D_{KL}[\mathbb{P}_{v_i} || \mathbb{P}_{z_i}]] \\ & + \sum_{i \in n} \mathbb{E}_{v_i \sim E_{\theta}(v_i | x)} \mathbb{E}_{z_i \sim E_{\phi}(z_i | v_i)} [D_{KL}[\mathbb{P}_{z_{\{1, \dots, n\}}} || \mathbb{P}_{z_{\{1, \dots, n\}/i}}]]. \end{aligned} \quad (9)$$

Here, θ and ϕ denote the parameters of the encoder and information bottleneck, respectively. In general, the first KL-divergence in Eq. (9) accounts for sufficiency, while the other one is utilized to promote consistency. Specifically, reducing $D_{KL}[\mathbb{P}_{v_i} || \mathbb{P}_{z_i}]$ can eliminate the task-irrelevant nuisances and simultaneously maximize $I(y; z_i)$. On the other hand, minimizing $D_{KL}[\mathbb{P}_{z_{\{1, \dots, n\}}} || \mathbb{P}_{z_{\{1, \dots, n\}/i}}]$ enables us to approximate I_i^c to its upper bound (i.e., $I(y; z_i)$) and thereby equivalently remove the view-specific information.

We elaborate the resulting framework in Fig. 3, where we demonstrate the process of eliminating both task-irrelevant and view-specific information.

Discussion. Notice the MV²D framework is essentially an extension of the information bottleneck architecture to the general multi-view learning, which reformulates the classic Lagrangian $I(V; Z) - I(Y; Z)$ as two terms of KL-divergence. Compared with other variants involving multiple views, domains, or modals learning [5], [6], [36], [7], the primary advantages of MV²D can be summarized as follows: (i) It ensures predictive and compact representations without computing any mutual information; (ii) It can accurately prioritize and purify the consistent information, which significantly improves the robustness to multi-view data. Proofs and detailed analysis of the advanced properties can be found in the Appendix.

4.2 Example1 (Single-view): Variational Self-Distillation

In this section, we present a special case of MV²D to produce optimal representations within single viewpoint, which obtains an analytical solution to fitting the mutual information between an input v and its representation z , namely Variational Self-Distillation (VSD) based on its formulation. Specifically, we first have $I(v; z)$ decomposed as:

$$I(v; z) = \underbrace{I(z; y)}_{\text{predictive}} + \underbrace{I(v; z|y)}_{\text{superfluous}}. \quad (10)$$

As illustrated by Fig. 1, an optimal representation requires maximization of $I(z; y)$ (*i.e.*, sufficiency) and elimination of $I(v; z|y)$ (*i.e.*, minimality). To this end, we reformulate Eq. (10) based on the data processing inequality $I(z; y) \leq I(v; y)$:

$$I(v; z) \leq I(v; y) + I(v; z|y), \quad (11)$$

which reforms the objective of an information bottleneck as: maximizing $I(v; y)$, minimizing $I(v; y) - I(z; y)$ and minimizing $I(v; z|y)$. Obviously, maximizing $I(v; y)$ is strictly consistent with the specific task and the last two terms are equivalent. Hence, the optimization is simplified to:

$$\min I(v; y) - I(z; y), \quad (12)$$

which tackles the prediction-compression trade-off and can be equivalently achieved by Eq. (13) based on Theorem 1 and Corollary 1. Formally, VSD maximizes the predictive information while concurrently minimizing the task-irrelevant nuisances through:

$$\mathcal{L}_{VSD} = \min_{\theta, \phi} \mathbb{E}_{v \sim E_{\theta}(v|x)} [\mathbb{E}_{z \sim E_{\phi}(z|v)} [D_{KL}[\mathbb{P}_v || \mathbb{P}_z]]], \quad (13)$$

where θ and ϕ denote the parameters of an encoder and information bottleneck, respectively. $\mathbb{P}_z = p(y|z)$, $\mathbb{P}_z = p(y|z)$ are the predictions, and D_{KL} represents the KL-divergence.

Compared with other IB strategies [4], [11], [16], VSD simultaneously achieves both sufficiency and minimality without estimating mutual information, demonstrating superior scalability and flexibility.

4.3 Example2 (Cross-view): Variational Cross Distillation and Variational Mutual Distillation

To deal with typical cross-view issues (*e.g.*, LiDAR-RGB, infrared-visible), we introduce another two variations of the MV²D, *i.e.*, Variational Cross Distillation (VCD) and Variational Mutual Distillation (VMD). Consider v_1 and v_2 as inputs from different modalities, and z_1, z_2 are the corresponding representations. VCD and VMD aim to neutralize the modal-discrepancies by eliminating both modal-specific and task-irrelevant information. More specifically, we first have the mutual information between z_1 and v_1 decomposed as follows (vice versa for z_2 and v_2):

$$I(v_1; z_1) = I(v_1; z_1|v_2) + I(v_2; z_1), \quad (14)$$

$$I(v_2; z_1) = I(v_2; z_1|y) + I(v_2; z_1; y). \quad (15)$$

As previously introduced, $I(v_1; z_1|v_2)$ represents that, the information contained in z_1 is unique to v_1 and is not accessible to v_2 , *i.e.*, modal-specific information, and $I(z_1; v_2)$

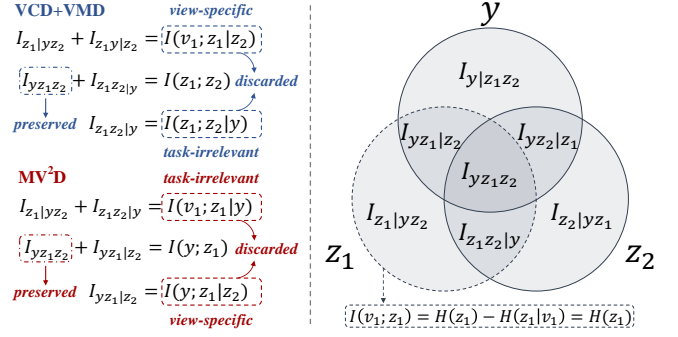


Fig. 4: Venn diagram in the right half is utilized for describing the mutual information among two representations z_1, z_2 and the target y . Left part demonstrates the proof skeleton to Sec. 4.4 from the view of mutual information.

denotes the information shared by z_1 and v_2 , which is named as modal-consistent information. On the other hand, $I(v_2; z_1|y)$ denotes the irrelevant information encoded in z_1 regarding given task [5], *i.e.*, superfluous information. Combining Eq. (15) with Eq. (14), we have:

$$I(v_1; z_1) = \underbrace{I(v_1; z_1|v_2)}_{\text{modal-specific}} + \underbrace{I(v_2; z_1|y)}_{\text{superfluous}} + \underbrace{I(v_2; z_1; y)}_{\text{predictive}}. \quad (16)$$

On this basis, VMD and VCD are applied to eliminate $I(v_1; z_1|v_2)$ and $I(v_2; z_1|y)$ respectively through:

$$\mathcal{L}_{VMD} = \min_{\theta, \phi} \mathbb{E}_{v_1, v_2 \sim E_{\theta}(v|x)} \mathbb{E}_{z_1, z_2 \sim E_{\phi}(z|v)} [D_{KL}[\mathbb{P}_{z_1} || \mathbb{P}_{z_2}]], \quad (17)$$

$$\mathcal{L}_{VCD} = \min_{\theta, \phi} \mathbb{E}_{v_1, v_2 \sim E_{\theta}(v|x)} \mathbb{E}_{z_1, z_2 \sim E_{\phi}(z|v)} [D_{KL}[\mathbb{P}_{v_2} || \mathbb{P}_{z_1}]]. \quad (18)$$

Here, θ and ϕ also denote the parameters of an encoder and information bottleneck architecture, and $\mathbb{P}_{z_1} = p(y|z_1)$, $\mathbb{P}_{v_2} = p(y|v_2)$ are the predicted distributions. Note Eq. (17) and Eq. (18) are symmetrically conducted to z_2 and v_2 to eliminate $I(v_2; z_2|v_1)$ and $I(v_1; z_2|y)$ respectively.

In essence, both VCD and VMD are special cases of MV²D when the total of viewpoints is two. It is noteworthy that they show remarkable scalability and flexibility when applying to various cross-modal issues with large-scale datasets, further demonstrating the effectiveness of MV²D in diverse circumstances. Next, we reveal the connections between MV²D and its variations.

4.4 Connections between Different Variations

Consider two special cases, where only one or two viewpoints are involved. For $n = 1$, apparently $I(y; z) = I^c$, and Eq. (9) degenerates to VSD. For $n = 2$, suppose z_1, z_2 are two representations corresponding to v_1 and v_2 , both of which are two observations of the same object x from two viewpoints. For better illustration, we first utilize the Venn diagram describing the mutual information among z_1, z_2, y in Fig. 4, and give our proof as follows.

Recall the chain rule [5], [35], [38], we have:

$$\begin{aligned} I(v_1; z_1) &= I(v_1; z_1|z_2) + I(z_2; z_1) \\ &= I(v_1; z_1|z_2) + I(z_2; z_1|y) + I_1^c. \end{aligned} \quad (19)$$

Revising the order of the chain, we have:

$$\begin{aligned} I(v_1; z_1) &= I(v_1; z_1|y) + I(y; z_1) \\ &= I(v_1; z_1|y) + I(y; z_1|z_2) + \hat{I}_1^c, \end{aligned} \quad (20)$$

in which we use hatted symbols to distinguish consistent information preserved by VCD, VMD and MV²D. Based on the definition of conditional mutual information, we have:

$$I(v_1; z_1|z_2) = H(z_1|z_2), \quad (21)$$

$$I(z_2; z_1|y) = H(z_1|y) - H(z_1|z_2, y). \quad (22)$$

Similarly, we have the following decomposition for Eq. (19):

$$I(v_1; z_1|y) = H(z_1|y), \quad (23)$$

$$I(y; z_1|z_2) = H(z_1|z_2) - H(z_1|z_2, y). \quad (24)$$

Note both $H(z_1|v_1, z_2)$ and $H(z_1|v_1, y)$ equals to zero based on the data processing inequality, thus they are omitted for simplicity. Combining Eq. (19)-Eq. (24), we conclude that I_1^c are equivalent to \hat{I}_1^c , indicating Eq. (9) degenerates to Eq. (18) and Eq. (17) when the total of viewpoints is two.

In the view of above, we introduce the following theory to reveal the connections between MV²D and its variations.

Corollary 2. *VSD, VCD and VMD are special cases of the proposed Multi-View Variational Distillation, in which there are only one or two views are involved.*

5 APPLICATIONS

In this section, we show the proposed variational distillation framework could be flexibly applied to various multi-modal/multi-view representation learning tasks: (i) Visible-Infrared Person Re-identification; (ii) Multi-view Classification; (iii) LiDAR-Image Semantic Segmentation. The quantitative and qualitative results demonstrate the effectiveness of our approach in various circumstances (*e.g.*, single-view, cross-view and multiple-view).

5.1 Cross-Modal Person Re-identification

We first evaluate our approach on Visible-Infrared Person Re-identification task. In this application, there are two kinds of images from different modals (*i.e.*, infrared and visible), and the objective is to match the target person images among a gallery of images when given a query image from another modal. The key challenge of this task hence lies in the huge heterogeneous gap between the visible and infrared images, which requires both complementary and consistent information to facilitate cross-modal retrieval. To verify the effectiveness of MV²D framework, we also design an intermediate modality by transforming both kinds of images to a new uniform image representation (see Fig. 6).

5.1.1 Evaluation Protocol and Benchmarks

In this section, we introduce the adopted benchmark datasets and corresponding evaluation standards. We follow the popular protocol [46], [45] for evaluation, where both cumulative match characteristic (CMC) and mean average precision (mAP) are used.

SYSU-MM01 [46] is collected from 6 cameras of both indoor and outdoor environments. It contains 287, 628 visible

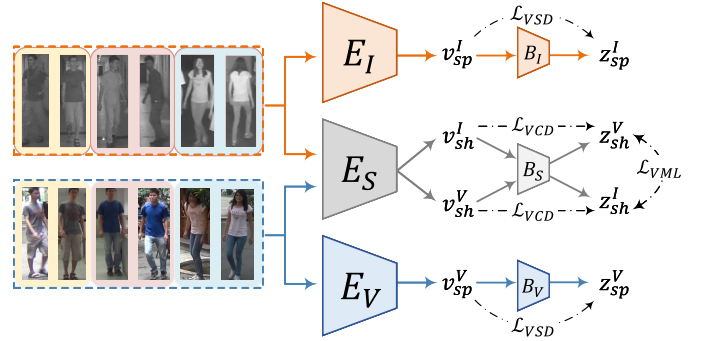


Figure 5: Network architecture for Multi-Modal Re-ID. $E_{I/S/V}$ and $B_{I/S/V}$ represent the encoder (ResNet-50) and information bottleneck (multi-layer perceptrons), respectively. v and z denote the observations and representations from encoder and information bottleneck, respectively

images and 15, 792 infrared images of 491 different persons in total, each of which is at least captured by two cameras. There are two search modes on SYSU-MM01, *i.e.*, all-search mode and indoor-search mode, and the difference lies in whether the outdoor cameras are excluded from the gallery.

RegDB [47] is collected from two aligned cameras (one visible and one infrared) and it totally includes 412 identities, where each identity has 10 infrared images and 10 visible images. Following the experimental protocol in [47], we divide the dataset into training and test sets randomly, each of which includes non-overlapping 206 identities. We test our model in both visible-to-thermal and thermal-to-visible settings. The final reported results are averaged over 10 trials with different training/test splits.

5.1.2 Implementation Details

Critical Architectures. For both MM01 and RegDB, we deploy three parallel branches, each of which is composed of a ResNet50 backbone (*i.e.*, encoder E_θ) and an information bottleneck (*i.e.*, E_ϕ : multi-layer perceptrons of 2 hidden ReLU units of size 1, 024 and 512 respectively with an output of size 2×256 that parameterizes mean and variance). In particular, we use two parallel modal-specific branches equipped with VSD to handle single modal image, and the remaining one (*i.e.*, modal-shared branch) takes cross-modal images as input, trained with VCD and VMD to produce consistent representations. For each branch, the backbone first encodes the input image to 2048-D feature (*i.e.*, observation v), then it is forwarded to the information bottleneck to obtain the compressed representation z . See Fig. 5 for the illustration of our ReID framework.

Moreover, we design another uniform image representation in addition to the default visible and infrared ones (see Fig. 6 for illustration). On this basis, the modal-shared branch takes inputs from three different viewpoints and adopts MV²D to further investigate the effectiveness in 3-view circumstance (please refer to the supplementary materials for more details).

Training. Following [43], [41], [42], we adopt the strong baseline with various training tricks, *i.e.*, warm up (linear scheme for first 10 epochs) and label smooth. We utilize the rank loss [48] for Re-ID learning, and set the weights of

TABLE 2: Performance of the proposed method compared with state-of-the-arts. Note that all methods are measured by CMC and mAP on SYSU-MM01. [introduce 2-view](#) and [3-view](#).

Settings			All Search				Indoor Search			
Type	Method	Venue	Rank-1	Rank-10	Rank-20	mAP	Rank-1	Rank-10	Rank-20	mAP
Generative	Hi-CMD [39]	CVPR'20	34.94	77.58	-	35.94	-	-	-	-
Network Design	DDAG [40]	ECCV'20	54.75	90.39	95.81	53.02	61.02	94.06	98.41	67.98
Network Design	NFS[41]	CVPR'21	56.91	91.34	96.52	55.45	62.79	96.53	99.07	69.79
Metric Design	MCLNet [42]	CVPR'21	65.40	93.33	97.14	61.98	72.56	96.98	99.20	76.58
Network Design	SMCL[43]	ICCV'21	67.39	92.87	96.76	61.78	68.84	96.55	98.77	75.56
Network Design	CM-NAS [44]	ICCV'21	61.99	92.87	97.25	60.02	67.01	97.02	99.32	72.95
Network Design	CMAAlign [26]	ICCV'21	55.41	-	-	54.14	58.46	-	-	66.33
Network Design	AGW [45]	TPAMI'21	47.50	84.39	92.14	47.65	54.17	91.14	95.98	62.97
Representation	ours (baseline)	-	64.15	94.42	98.68	61.74	69.61	95.78	98.90	75.15
Representation	ours (2-view)	-	70.02	96.17	98.76	66.70	78.26	97.87	99.72	81.79
Representation	ours (3-view)	-	71.65	96.26	98.71	67.95	79.08	99.00	99.91	81.84

TABLE 3: Comparison with the state-of-the-arts on RegDB dataset under visible-thermal and thermal-visible settings.

Settings		Visible2Thermal		Thermal2Visible	
Method	Venue	Rank-1	mAP	Rank-1	mAP
Hi-CMD [39]	CVPR'20	70.9	66.0	-	-
DDAG [40]	ECCV'20	69.3	63.5	68.1	61.8
NFS [41]	CVPR'21	80.5	72.1	77.9	69.8
MCLNet [42]	CVPR'21	80.3	73.1	75.9	69.5
CMAAlign [26]	ICCV'21	67.6	74.2	65.5	65.9
AGW [45]	TPAMI'21	70.1	66.4	70.5	72.4
ours (baseline)	-	79.9	77.2	77.5	76.2
ours (2-view)	-	81.6	78.7	79.1	77.5
ours (3-view)	-	83.1	80.1	81.2	78.4

cross-entropy, rank loss and variational distillation objective to 1, 1, 2, respectively. All experiments are optimized by Adam optimizer with an initial learning rate of 2.6×10^{-4} , which then decays 10 times at 200 epochs in total of 300. Horizontal flip and normalization are utilized to augment the training images, where the images are resized to 288×144 . The batch size is set to 64 for all experiments, in which it contains 8 different identities, and each identity includes 4 RGB images and 4 IR images.

5.1.3 Experimental Results

Comparison. As shown in Tab. 2 and Tab. 3, our approaches outperform all competitors by a large margin on both datasets. Moreover, compared with our baseline model, the proposed MV²D significantly boosts the performance in both 2-view and 3-view cases, demonstrating its effectiveness and generalization ability. It is also noteworthy that our optimization is quite efficient since the estimation of mutual information is avoided (see complexity comparison in Tab. 5). Since the additional viewpoint is not provided in the benchmarks by default, the following experiments are conducted only on the infrared and visible images.

Ablation Study. We first clarify different settings in Tab. 4, where “ E_S ” and “ $E_{I/V}$ ” denote whether we use the modal-shared branch and modal-specific branches. “ B_S ” and “ $B_{I/V}$ ” indicate that whether we utilize the information bottleneck architecture in each branch. “CIB” denotes we adopt the conventional IB for training. “VSD”, “VMD” and

Figure 6: Illustrative examples of the adopted viewpoints in 3-view experiments.



“VCD” denote our approaches, and are uniformly represented with “VD” when applying all of them. Based on Tab. 4, we have the following observations:

(i) Information bottleneck architecture can improve the performance in both single-view, cross-view and triple-view cases (see 3rd, 7th and 11th row in Tab. 4).

(ii) It seems that conventional IB strategy has no advantages in learning predictive information (see 2nd, 6th and 10th row in Tab. 4). We conjecture it is because, by explicitly reducing $I(v; z)$, conventional IB may not recognize label information from task-irrelevant distractors, and probably discard all of them. On the other hand, estimation of mutual information in high dimension is difficult, especially when involving multi-modal data and latent variables in our setting, which leads to a sharp drop to performance.

(iii) Our approach provides remarkable improvement under various settings (see 4th, 8th and 12th row in Tab. 4). In single-view case, by maximally preserving predictive information while simultaneously reducing superfluous details, VSD outperforms the conventional IB by 27.68%@Rank-1 and 24.58%@mAP (comparing 8th with 6th row in Tab. 4). In cross-view case, VCD and VMD achieve 23.14%@Rank-1 and 22.82%@mAP improvement against the conventional IB (see 4th and 2nd row in Tab. 4), demonstrating huge advantages as well.

Sufficiency & Consistency. For better illustration, we plot the 2D projection of the representations by using t-SNE on Fig. 7 and Fig. 8, where we compare our approach with the conventional IB. In particular, z_{sp} and z_{sh} denote the representations obtained from the modal-specific

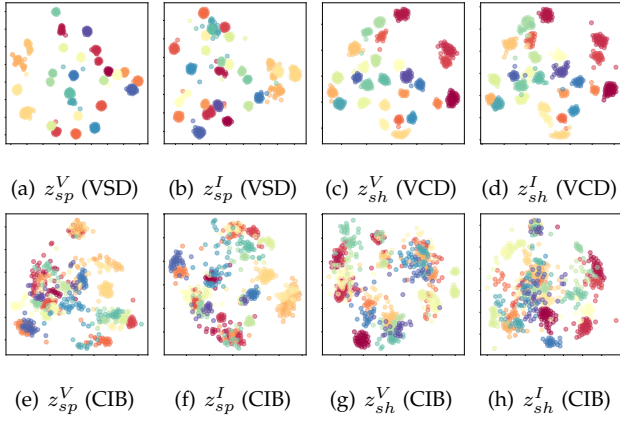


Figure 7: 2-D projections of the embedding space by using t-SNE. The results are obtained from our method and conventional IB on SYSU-MM01 test set. Different colors are used to represent different person IDs.

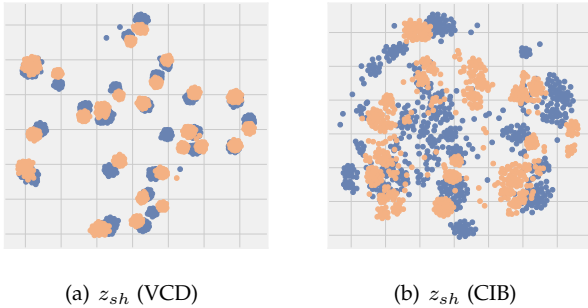


Figure 8: 2D projections of the joint embedding spaces of z_{sh}^I and z_{sh}^V obtained by using t-SNE on SYSU-MM01.

branches and the modal-shared branch respectively, and the superscripts I and V indicate the corresponding inputs are infrared or visible. Based on Fig. 7 and Fig. 8, we have:

(i) As shown in Fig. 7(e)~7(h), the embedding space of conventional IB is mixed, demonstrating the inferior predictive power and severe redundancy of the learned representation. On the contrary, our method shows evident boost to the discriminative ability with clear class boundaries (see Fig. 7(a)~7(d)).

(ii) From Fig. 7(g), 7(h) and 8(b), we observe the conventional IB is quite vulnerable and sensitive to modal changes, where we can find the discrepant embedding spaces from different modalities. Such phenomenon is not surprising since conventional IB cannot explicitly distinguish modal-consistent/specific information. By contrast, the embedding space of z_{sh}^I and z_{sh}^V obtained from our method appears to coincide with each other (see Fig. 7(c), 7(d) and 8(a)), implying that we can learn a consistent representation.

Complexity. We also compare the extra computational and memory cost brought by our method and conventional IB. As shown in Tab. 5, “**Enc**” denotes the encoder, *i.e.*, backbone network, “**IB**” and “**MIE**” represents the information bottleneck architecture and mutual information estimator. Clearly, our approach avoids explicit calculation to Eq. (3),

TABLE 4: Accuracy of our method when using different training strategies. Note all experiments are conducted on SYSU-MM01 under all-search single-shot mode.

Settings	R1	R10	R20	mAP
1 E_S	53.19	88.19	94.69	49.16
2 [†] E_S+CIB	38.02	74.68	83.85	37.94
3 E_S+B_S	56.95	93.11	97.66	57.01
4 $E_S+B_S+VCD+VMD$	61.16	94.61	97.97	60.76
5 $E_{I/V}$	57.61	93.68	97.68	56.24
6 [†] $E_{S/I/V}+CIB$	41.65	79.65	88.77	41.69
7 $E_{I/V}+B_{I/V}$	62.26	95.08	98.79	59.27
8 $E_{I/V}+B_{I/V}+VSD$	69.33	95.71	98.63	66.27
9 $E_{S/I/V}$	58.60	93.59	97.83	57.35
10 [†] $E_{S/I/V}+CIB$	43.81	82.91	92.82	41.77
11 $E_{S/I/V}+B_{S/I/V}$	64.15	94.42	98.68	61.74
12 $E_{S/I/V}+B_{S/I/V}+VD$	70.02	96.17	98.76	66.70

[†] Some results are compared for completeness, as conventional IB does not explicitly enforce any constraints to the observation.

Method	Enc	IB	MIE	Time	Params
Baseline	✓			1.0x	1.0x
Ours	✓	✓		1.09x	1.15x
CIB	✓	✓	✓	1.26x	1.35x

TABLE 5: Computational cost of different methods.

and thus implement IB principle with negligible cost.

5.2 Multi-View Classification

Multi-view classification aims to optimally integrate various representations from different visual views to improve classification accuracy. “Multi-view” in this context means every object is described by different descriptors, and hence there exists a pre-extracted feature set including heterogeneous features with tremendous diversity and complementary information. This scenario therefore is satisfactory to valid the effectiveness of our MV²D (multiple views cases), which allows the network to promote both sufficiency and view-consistency.

5.2.1 Evaluation Protocol and Benchmarks

Following [1], [2], [28], the adopted multi-view benchmark datasets are split into three parts (*i.e.*, 70%/20%/10%) for training, validation and testing, respectively. Classification accuracy is utilized as the prominent evaluation metric for conducting comparisons with the state-of-the-art techniques.

Caltech-101/20 [49] consists of 101 categories of images. Following [50], [28], we select the widely used 2386 images of 20 classes and 9144 images of 102 classes (101 object categories and an additional background class), respectively, denoted as Caltech-20 and Caltech-101. This dataset provides 6 kinds of pre-extracted features for each image, *i.e.*, 48-D Gabor, 40-D Wavelet moments, 254-D CENTRIST, 1984-D HOG, 512-D GIST, and 928-D LBP.

AWA [51] is composed of 30, 475 images of 50 different animals with 6 heterogeneous pre-extracted features for

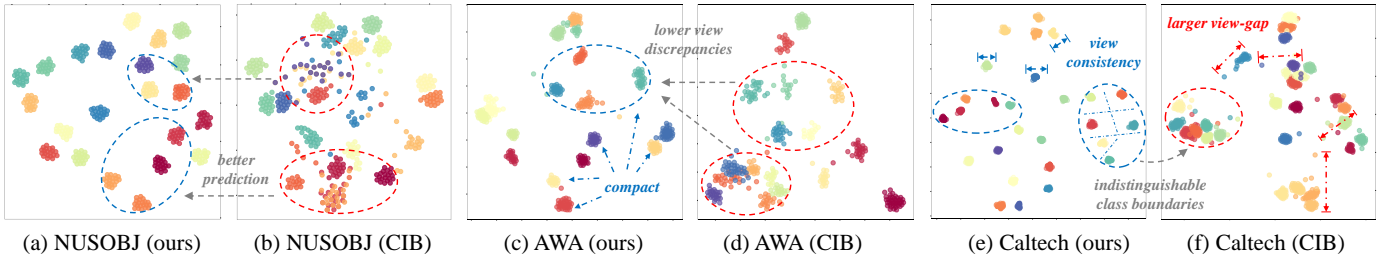


Figure 9: 2D projections of the embedding obtained applying MV^2D and conventional IB strategy to the NUSOBJ, AWA, Caltech datasets. The representation is projected onto the two principal components, where different colors are used to represent various categories.

Method	Cal101	Cal20	AWA	NUS	Reuters	Hand
SVMcon [55]	47.90	83.83	31.04	42.72	88.18	97.67
DeepLDA [56]	45.65	76.51	25.60	20.32	84.91	97.67
MvDA [27]	45.20	76.28	9.79	11.46	78.83	21.33
DCCA [1]	66.18	86.50	20.68	28.75	64.92	91.60
DCCAE[2]	26.89	50.27	13.48	27.48	56.53	80.00
GradKCCA [57]	50.53	92.92	33.33	48.15	43.39	95.74
MvNNcor[28]	76.00	97.92	47.69	52.05	89.28	99.48
CPM-Nets [58]	83.22	98.23	54.38	57.39	93.10	99.56
ours (baseline)	82.66	96.87	54.04	58.45	93.06	99.29
ours	85.93	99.16	56.25	59.60	95.46	99.40

TABLE 6: Comparison to the state-of-the-arts on multi-view classification datasets, where the results are obtained using the average of five experiments.

each image. Specifically, they are 2688-D Color Histogram, 2000-D Local Self-Similarity, 252-D Pyramid HOG, 2000-D SIFT, 2000-D color SIFT, and 2000-D SURF.

NUSOBJ [52] is a subset of NUS-WIDE and contains 31 object categories and 30,000 images in total. It has 5 types of low-dimensional features extracted from all images, including 64-D color histogram, 225-D block-wise color moments, 144-D color correlogram, 73-D edge direction histogram, and 128-D wavelet texture.

Reuters [53] is a document dataset collected from 5 different languages. It contains 18,758 documents in total, all of which are uniformly categorized into 6 classes. Note different languages can be seen as different views, that is, English (21, 531-D), French (24, 892-D), German (34, 251-D), Italian (15, 506-D) and Spanish (11547-D).

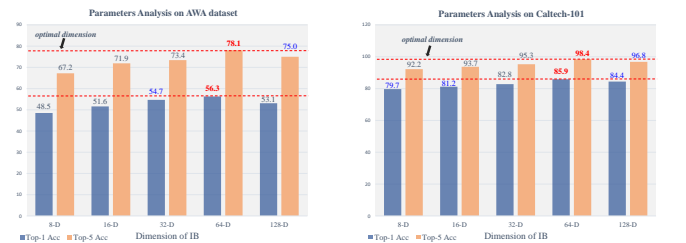
Hand [54] consists of features of handwritten numerals extracted from a collection of Dutch utility maps, 200 patterns per categories (a total of 2000 patterns). These digits are represented in terms of 6 feature sets, containing 76-D Fou, 216-D Fac, 64-D Kar, 240 Pix, 47-D Zer, and 6-D Mor.

5.2.2 Implementation Details

Critical Architectures. We choose MvNNcor [28] as our baseline, which is composed of two parts, *i.e.*, a set of neural networks $\{f_i\}_{i=1}^M$ (*i.e.*, the encoder E_θ in Fig. 3), and an auxiliary module $\{f_\psi\}$. Formally, M denotes the total number of viewpoints and each f_i is a fully-connected network consisting of d_i input units and two hidden layers with 512 and 256 units equipped with ReLU activation function. To implement MV^2D , we append an information bottleneck architecture to each f_i referred to Fig. 3, where we omit f_ψ for simplicity (more details can be found in A.3 in the supplementary material).

Settings	Cal101	Cal20	AWA	NUS	Reuters	Hand
E_θ	81.28	94.66	53.51	57.79	91.69	99.20
$E_\theta + CIB$	64.29	81.16	37.90	45.88	74.39	87.53
$E_\theta + E_\phi$	82.66	96.87	54.04	58.45	93.06	99.29
$E_\theta + E_\phi + MV^2D$	85.93	99.16	56.25	59.60	95.46	99.40

TABLE 7: Performance of our approach when adopting different settings.



(a) Accuracy on AWA with varying dimension of IB.

(b) Accuracy on Caltech with varying dimension of IB.

Figure 10: Analysis on the dimension of the information bottleneck. This evaluation is conducted on AWA and Caltech-101 datasets.

Training. We follow the same experimental configurations in [28], where all experiments are optimized by Adam with $\beta_1 = 0.5$ and $\beta_2 = 0.9$. The learning rate is initialized with 10^{-3} and decays 20 times at 30-th and 60-th epoch. All networks are trained from scratch with a batch size of 64, and are updated with 160 epochs in total. The training objective includes three terms, *i.e.*, classification loss, rank loss and Eq. (9).

5.2.3 Experimental Results

Comparison. Tab. 6 and Tab. 7 summarize the quantitative results on multi-view classification. Due to the rank metric learning, we obtain a relatively stronger baseline compared with MvNNcor, and MV^2D achieves a significant improvement beyond this baseline on all benchmark datasets. Compared with SOTA CCA-based methods [1], [2], [57], our method also demonstrates promising advantages on the classification performance (*e.g.*, outperforms [57] by 35.4% on Caltech101). The improvement brought by MV^2D can be mostly attributed to the accurate elimination of both non-predictive and view-specific information, which neutralizes sensitivity to view-changes. On the other hand, we also observe our information-theoretic constraint drives the deep models [28], [58], [56] to learn the sufficient and con-

TABLE 8: Quantitative results of different approaches on nuScenes_lidarseg validation set.

Methods	mIoU(%)	barrier	bicycle	bus	car	construction	motorcycle	pedestrian	traffic_cone	trailer	truck	driveable	other_flat	sidewalk	terrain	manmade	vegetation
RangNet++ [59]	65.5	66.0	21.3	77.2	80.9	30.2	66.8	69.6	52.1	54.2	72.3	94.1	66.6	63.5	70.1	83.1	79.8
SPVCNN [60]	67.8	67.1	12.0	80.0	89.2	34.8	63.5	70.0	47.0	48.5	76.4	93.6	58.6	67.8	72.6	86.5	85.4
PolarNet [61]	71.0	74.7	28.2	85.3	90.9	35.1	77.5	71.3	58.8	57.4	76.1	96.5	71.1	74.7	74.0	87.3	85.7
Cylinder3D [62]	76.1	76.4	40.3	91.4	93.8	51.3	78.0	78.9	64.9	62.1	84.4	96.8	71.6	76.4	75.4	90.5	87.4
AF2S3Net [63]	78.3	78.9	52.2	89.9	84.2	77.4	74.3	77.3	72.0	83.9	73.8	97.1	66.5	77.5	74.0	87.7	86.8
PMF [64]	76.9	74.1	46.6	89.8	92.1	57.0	77.7	80.9	70.9	64.6	82.9	95.5	73.3	73.6	74.8	89.4	87.7
ours (baseline)	77.2	74.7	47.1	90.0	92.3	58.1	80.1	81.4	68.6	62.0	81.9	95.6	73.7	73.6	75.8	90.4	89.2
ours	78.9	75.5	55.8	93.8	91.7	61.2	83.4	84.0	74.2	63.2	81.3	95.4	74.2	73.2	75.1	90.6	89.4

TABLE 9: Quantitative results of different approaches on SemanticKITTI validation set.

Methods	mIoU(%)	road	sidewalk	parking	other ground	building	car	truck	bicycle	motorcycle	other vehicle	vegetation	trunk	terrain	person	bicyclist	motorcyclist	fence	pole	traffic-sign
RandLANet [65]	50.0	90.7	73.7	60.2	20.4	86.9	94.2	40.1	26.0	25.8	38.9	81.4	66.8	49.2	49.2	48.2	7.2	56.3	47.7	38.1
SPVCNN[60]	58.7	90.2	75.4	67.6	21.8	91.6	97.2	56.6	50.6	50.4	58.0	86.1	73.4	71.0	67.4	67.1	50.3	66.9	64.3	67.3
PolarNet [61]	54.3	90.8	74.4	61.7	21.7	90.0	93.8	22.9	40.3	30.1	28.5	84.0	65.5	67.8	43.2	40.2	5.6	61.3	51.8	57.5
BAAF-Net [66]	59.9	90.9	74.4	62.2	23.6	89.8	95.4	48.7	31.8	35.5	46.7	82.7	63.4	67.9	49.5	55.7	53.0	60.8	53.7	52.0
JS3C-Net [67]	66.0	88.9	72.1	61.9	31.9	92.5	95.8	54.3	59.3	52.9	46.0	84.5	69.8	67.9	69.5	65.4	39.9	70.8	60.7	68.7
PMF [64]	63.9	96.4	80.5	43.5	0.1	88.7	95.4	68.4	71.6	0.0	75.2	88.6	72.7	75.3	78.9	71.6	0.0	60.1	65.5	43.0
ours (baseline)	64.7	94.7	75.8	55.6	14.1	89.4	96.2	53.9	55.7	50.0	52.5	86.4	67.8	70.4	63.9	69.2	42.5	63.3	60.4	68.1
ours	66.5	95.9	77.4	60.3	17.9	91.6	96.4	59.1	56.8	51.6	53.5	87.2	69.7	71.4	66.3	70.5	46.4	64.7	60.2	69.8

sistent representations, by achieving stronger performance without requiring complex designs.

Ablation Study. Based on the Tab. 7, we can draw the similar conclusions in multi-view case: (i) The appended IB architecture can improve the performance as it introduces additional parameters; (ii) Conventional IB strategy still has no benefits in promoting the accuracy under multi-view cases; (iii) MV²D can evidently boost the performance on all datasets but excluding Hand [54]. The reason might be the dimension of feature in this dataset is only 6, which can hardly include rich sources of information. Such phenomenon also reveals the shortcomings of MV²D, *i.e.*, incapability to choose the optimal dimension, and becoming mediocre when handling fairly low-dimensional objects.

Analysis on Feature Dimension of IB. As is shown in Fig. 10, the accuracy first climbs to a peak with the increase of output dimension of IB, and then degrades. We deduce there are two reasons accounting for this phenomenon: (i) necessary information would be inevitably discarded if the dimension is extremely reduced, which can be concluded from our inferior performance on Hand dataset; (ii) Compact representation are usually beneficial for the downstream tasks.

Sufficiency & Consistency. We also plot the 2D projection of representations by using t-SNE on Fig. 9, where we compare the representations obtained from our approach and conventional IB. By observing the scatters, we have: (i) The embedding space produced by CIB appear to lack

discrimination, where we can spot obvious overlapping within each class and indistinguishable boundaries between different categories; (ii) By contrast, almost all the clusters obtained by MV²D concentrate around a respective centroid, suggesting the sufficiency and view-consistency information are better preserved.

5.3 LiDAR-RGB Semantic Segmentation

In this section, we further evaluate the variational distillation framework on LiDAR-RGB semantic segmentation, which, in practice, is a typical cross-modal learning problem. It is a fundamental task for scene perception and understanding, which aims to predict a dense label map by fusing complementary information from both LiDAR and RGB sensors. Thus, it is also quite suitable to evaluate the variational distillation framework in such a scalable and complex representation learning problem.

5.3.1 Evaluation Protocol and Benchmarks

To evaluate the proposed method, we follow the official protocol [68], [69] to leverage mean intersection-over-union (mIoU) as the evaluation metric. For a given class i , IoU is formulated as: $IoU_i = TP_i / (TP_i + FP_i + FN_i)$, where TP_i , FP_i , FN_i represent true positive, false positive, and false negative predictions for the i -th class and the mIoU is the mean value of IoU over all classes.

nuScenes [68] collects 1000 scenes of 20s duration with 32 beams LiDAR sensor. The number of total frames is

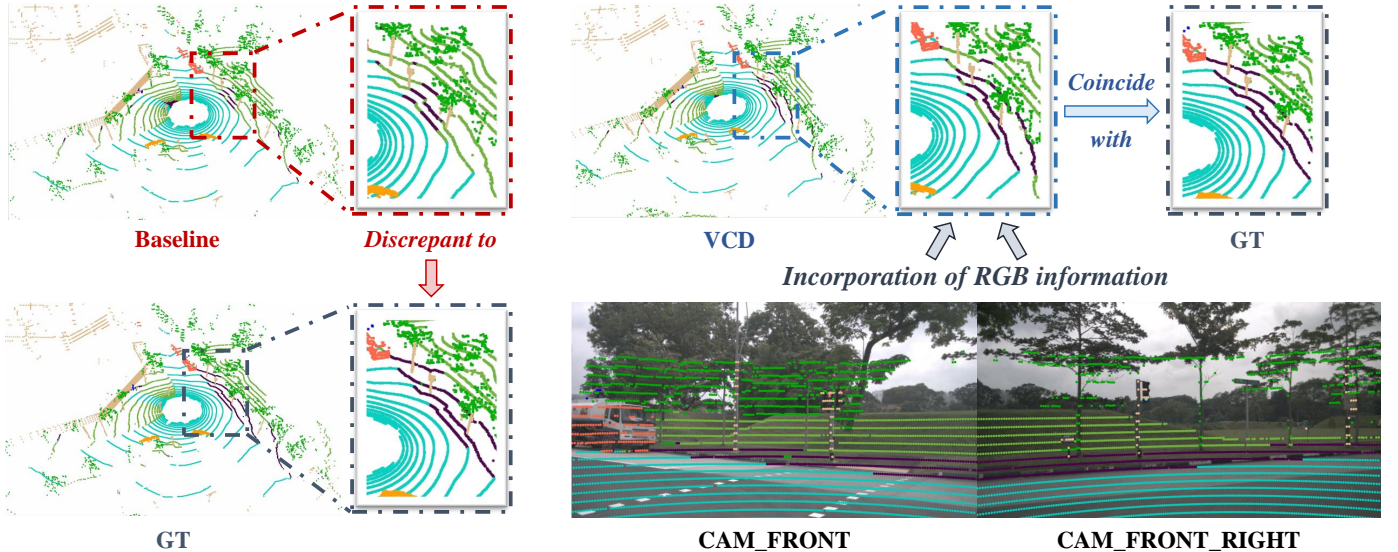


Figure 11: Qualitative results obtained from our baseline and VCD on nuScenes dataset, where different colors are utilized to denote various categories. Note the RGB images are taken from the front camera and the front-right camera, and provide crucial complementary information for the LiDAR-based segmentation.

40,000, and are split into 28,130 training frames and 6,019 validation frames. After merging similar classes and removing rare classes, total 16 classes for the LiDAR semantic segmentation are remained. Unlike SemanticKITTI, which provides only the images of the front-view camera, nuScenes has 6 cameras for different views of LiDAR.

SemanticKITTI [69] is a large-scale driving scene dataset for point cloud segmentation, which provides 43,000 scans with point-wise semantic annotation. This dataset consists of 22 sequences in total, splitting sequences 00 to 10 as training set (where sequence 08 is used as the validation set), and sequences 11 to 21 as test set. 19 classes are used for training and evaluation after ignoring and merging the classes with very few points or with different moving status.

5.3.2 Implementation Details

Critical Architectures. Our framework is mainly composed of two sub-networks to handle inputs from different modalities (*i.e.*, image and LiDAR), and each of which includes a backbone network (*i.e.*, E_θ) and an information bottleneck architecture to implement VCD. In addition, we also adopt a LI-fusion module [70] to enhance the LiDAR point representation by incorporating image features at multiple scales. More specifically, the image sub-network extracts the semantic information with a set of convolutional operations, which are implemented by SwiftNet [71] pretrained on ImageNet. We adopt SPVCNN [60] as the Point Cloud sub-network, which outputs the final representation for segmentation. Details and graphical illustration of our framework can be found in A.2 in the supplementary material.

Training. All experiments are optimized by SGD with Nesterov, where weight decay and momentum are set to 1×10^{-4} and 0.9, respectively. The learning rate starts at 2.4×10^{-1} and adopts the warm-up with cosine scheduler. We train our model for 40 epochs in total with batch size fixed to 8, and we conduct all experiments on NVIDIA RTX A6000 GPUs. In addition to the widely adopted cross-entropy, the

training objective also consists of multi-class focal loss [72], Lovász-softmax loss [73] and our VCD.

5.3.3 Experimental Results

Quantitative Analysis. Tab. 8 and Tab. 9 shows the comparison on the validation set of nuScenes and SemanticKITTI. We can draw the following conclusion: Our approach evidently boosts the performance and outperforms the baseline and other competitors in term of mIoU on both benchmark datasets. More specifically, the proposed variational distillation framework exceeds the SPVCNN [60] (our point cloud baseline) by a large margin, and it also demonstrates superiority to the projection-based [65], [61], [59], voxel partition and 3D convolutional methods [62], [66], [67], [63] on both datasets, revealing its effectiveness. Besides, since [63] and [67] adopt stronger baselines and various modules specifically designed for point cloud, the performance disparities are relatively inconspicuous compared with our method.

Qualitative Analysis. Fig. 11 provides a visual illustration to the produced labeling map. Obviously, VCD can better facilitate the fusion of complementary information and thus attains preferable segmentation result. By comparison, we observe some categories which are hardly recognized are ignored by the baseline, which shows IB can handle the huge modal-discrepancy.

6 CONCLUSION

In this work, we provide an analytical solution to fitting mutual information by using variational inference, rather than designing a sophisticated estimator. On this basis, we reformulate the objective of IB, and propose a generalized variational distillation framework, which enables us to jointly preserve the sufficiency of representations and get rid of task-irrelevant distractors. Its special

cases, *i.e.*, Multi-View Variational Distillation (MV²D), Variational Cross-Distillation (VCD) and Variational Mutual-Distillation (VMD), can produce view-consistent representations among multiple heterogeneous data observations. The future works would include learning an adaptive method to determine the output dimension of IB. Also, more broader multi-view applications such as medical and text would be studied.

APPENDIX A PROOF DETAILS

Given $\{v_1, v_2, \dots, v_n\}$ as n observations of the same object x from different viewpoints, domains, or modals, and let y be the ground-truth label. Consider $\{z_1, z_2, \dots, z_n\}$ to be the corresponding representations obtained from an information bottleneck, we make the following two simple assumptions:

Hypothesis:

(H_1) information shared by more views leads to better robustness

(H_2) no representations are only composed of view-specific information

Thesis:

(T_1) minimizing $D_{KL}[\mathbb{P}_{z_{\{1,\dots,n\}}} || \mathbb{P}_{z_{\{1,\dots,n\}/i}}]$ is consistent with the objective of eliminating view-specific information, which also complies with sufficiency constraint

(T_2) MV²D automatically and accurately prioritizes different compositions of the preserved information based on the generalization ability

A.1 Proof to Thesis 1

Consider z_i as the representation of v_i , we have the following factorization using the chain rule [5], [35]:

$$I(v_i; z_i) = \underbrace{I(y; z_i)}_{\text{predictive}} + \underbrace{I(v_i; z_i|y)}_{\text{superfluous}}. \quad (25)$$

Notice $I(y; z_i)$ is composed of various terms when multiple views are involved (see Fig. 2 for visualization). Hence, we have:

$$I(y; z_i) = \underbrace{I_i^c}_{\text{consistent}} + \underbrace{I(y; z_i|z_{\{1,\dots,n\}/i})}_{\text{view-specific}}, \quad (26)$$

where I_i^c is utilized to uniformly represent all compositions of the view-consistent information encoded in z_i , and $I(y; z_i|z_{\{1,\dots,n\}/i})$ denotes the information that is unique to z_i , and is inaccessible to all other representations, *i.e.*, view-specific information. Substituting Eq. (26) into Eq. (25), we have:

$$I(v_i; z_i) = \underbrace{I(v_i; z_i|y)}_{\text{superfluous}} + \underbrace{I(y; z_i|z_{\{1,\dots,n\}/i})}_{\text{view-specific}} + \underbrace{I_i^c}_{\text{consistent}}. \quad (27)$$

According to Definition 2, consistency requires to eliminate both $I(v_i; z_i|y)$ and $I(y; z_i|z_{\{1,\dots,n\}/i})$ while simultaneously

maximizing I_i^c . However, I_i^c includes multiple terms and is almost impossible to be directly optimized. To resolve this issue, we first introduce the following inequality based on the information processing principle:

$$I(v_i; z_i) \leq I(v_i; z_i|y) + I(y; z_i|z_{\{1,\dots,n\}/i}) + I(y; z_i), \quad (28)$$

which indicates promoting consistency undergoes several sub-processes: (i) maximizing $I(y; z_i)$; (ii) approximating I_i^c to its upper bound, *i.e.*, $I(y; z_i)$; (iii) discarding the task-irrelevant nuisances $I(v_i; z_i|y)$; (iv) eliminating view-specific information $I(y; z_i|z_{\{1,\dots,n\}/i})$.

To that end, the training objective can be formulated as:

$$\min \sum_{i \in n} \underbrace{I(v_i; z_i|y) - I(y; z_i)}_{\text{sufficiency}} + \underbrace{I(y; z_i|z_{\{1,\dots,n\}/i})}_{\text{consistency}}, \quad (29)$$

where, as elaborated in Sec. 4.1 and Sec. 4.2, the sufficiency term in Eq. (29) accounts for (i) and (iii), while the consistency term are utilized for (ii) and (iv).

Next, given $z_i \in \{z_1, \dots, z_n\}$, we have the view-specific information divided as follows [35], [38]:

$$\begin{aligned} I(y; z_i|z_{\{1,\dots,n\}/i}) &= H(y|z_{\{1,\dots,n\}/i}) - H(y|z_{\{1,\dots,n\}}) = \\ &= - \int p(y|z_{\{1,\dots,n\}/i}) \log p(y|z_{\{1,\dots,n\}/i}) dy \\ &+ \int p(y|z_{\{1,\dots,n\}}) \log p(y|z_{\{1,\dots,n\}}) dy = \\ &= - \int p(y|z_{\{1,\dots,n\}/i}) \log \left[\frac{p(y|z_{\{1,\dots,n\}/i})}{p(y|z_{\{1,\dots,n\}})} p(y|z_{\{1,\dots,n\}}) \right] dy \\ &+ \int p(y|z_{\{1,\dots,n\}}) \log \left[\frac{p(y|z_{\{1,\dots,n\}})}{p(y|z_{\{1,\dots,n\}/i})} p(y|z_{\{1,\dots,n\}/i}) \right] dy, \end{aligned} \quad (30)$$

in which $H(\cdot)$ represents Shannon entropy. By factorizing the first integral in Eq. (30), we obtain:

$$\begin{aligned} & \int p(y|z_{\{1,\dots,n\}/i}) \log \left[\frac{p(y|z_{\{1,\dots,n\}/i})}{p(y|z_{\{1,\dots,n\}})} p(y|z_{\{1,\dots,n\}}) \right] dy \\ &= \underbrace{\int p(y|z_{\{1,\dots,n\}/i}) \log \left[\frac{p(y|z_{\{1,\dots,n\}/i})}{p(y|z_{\{1,\dots,n\}})} \right] dy}_{\text{term } Z_1} \\ &+ \underbrace{\int p(y|z_{\{1,\dots,n\}/i}) \log p(y|z_{\{1,\dots,n\}}) dy}_{\text{term } Z_2}. \end{aligned} \quad (31)$$

Similarly, we have the second one divided as:

$$\begin{aligned} & \int p(y|z_{\{1,\dots,n\}}) \log \left[\frac{p(y|z_{\{1,\dots,n\}})}{p(y|z_{\{1,\dots,n\}/i})} p(y|z_{\{1,\dots,n\}/i}) \right] dy \\ &= \underbrace{\int p(y|z_{\{1,\dots,n\}}) \log \left[\frac{p(y|z_{\{1,\dots,n\}})}{p(y|z_{\{1,\dots,n\}/i})} \right] dy}_{\text{term } \hat{Z}_1} \\ &+ \underbrace{\int p(y|z_{\{1,\dots,n\}}) \log p(y|z_{\{1,\dots,n\}/i}) dy}_{\text{term } \hat{Z}_2}. \end{aligned} \quad (32)$$

Integrating term \mathbb{Z}_1 and term $\widehat{\mathbb{Z}}_1$ over y :

$$\mathbb{Z}_1 = D_{KL} [p(y|z_{\{1,\dots,n\}/i}) || p(y|z_{\{1,\dots,n\}})], \quad (33)$$

$$\widehat{\mathbb{Z}}_1 = D_{KL} [p(y|z_{\{1,\dots,n\}/i}) || p(y|z_{\{1,\dots,n\}/i})], \quad (34)$$

where $D_{KL}[\cdot || \cdot]$ denotes the relative entropy, *i.e.*, KL-divergence. Then we integrate term \mathbb{Z}_2 and term $\widehat{\mathbb{Z}}_2$ over y and show the following:

$$\mathbb{Z}_2 = -H(p(y|z_{\{1,\dots,n\}/i}), p(y|z_{\{1,\dots,n\}})), \quad (35)$$

$$\widehat{\mathbb{Z}}_2 = -H(p(y|z_{\{1,\dots,n\}}), p(y|z_{\{1,\dots,n\}/i})). \quad (36)$$

Obviously, both \mathbb{Z}_2 and $\widehat{\mathbb{Z}}_2$ are cross entropies.

Based on the above analysis, the view-specific information contained in $I(y; z_i | z_{\{1,\dots,n\}/i})$ can be represented with:

$$I(y; z_i | z_{\{1,\dots,n\}/i}) = -(\mathbb{Z}_1 + \mathbb{Z}_2) + (\widehat{\mathbb{Z}}_1 + \widehat{\mathbb{Z}}_2). \quad (37)$$

Using the non-negativity of entropies, we have

$$I(y; z_i | z_{\{1,\dots,n\}/i}) \leq D_{KL} [p(y|z_{\{1,\dots,n\}}) || p(y|z_{\{1,\dots,n\}/i})] + H(p(y|z_{\{1,\dots,n\}/i}), p(y|z_{\{1,\dots,n\}})). \quad (38)$$

Denoting $p(y|z_{\{1,\dots,n\}/i})$ and $p(y|z_{\{1,\dots,n\}})$ as \mathbb{P}_Z and $\widehat{\mathbb{P}}_Z$ for simplicity, we have the upper bound as:

$$\mathbb{E}_{v_i \sim E_\theta(v_i|x)} \mathbb{E}_{z_i \sim E_\phi(z_i|x)} \left[D_{KL}[\widehat{\mathbb{P}}_Z || \mathbb{P}_Z] + H(\mathbb{P}_Z, \widehat{\mathbb{P}}_Z) \right], \quad (39)$$

where θ and ϕ parameterize the encoder and the information bottleneck. In the view of above, the objective of eliminating view-specific information can be formalized as:

$$\min_{\theta, \phi} \mathbb{E}_{v_i \sim E_\theta(v_i|x)} \mathbb{E}_{z_i \sim E_\phi(z_i|x)} \left[D_{KL}[\widehat{\mathbb{P}}_Z || \mathbb{P}_Z] + H(\mathbb{P}_Z, \widehat{\mathbb{P}}_Z) \right]. \quad (40)$$

Clearly, the objective of eliminating view-specific information is consistent with reducing the discrepancy between \mathbb{P}_Z and $\widehat{\mathbb{P}}_Z$. Notice this can be attained by minimizing $D_{KL}[\widehat{\mathbb{P}}_Z || \mathbb{P}_Z]$ only, which approximates \mathbb{P}_Z to $\widehat{\mathbb{P}}_Z$ and forces E_ϕ to focus more on the view-consistent information, preventing explicit violation to the sufficiency constraint. Ideally, $D_{KL}[\widehat{\mathbb{P}}_Z || \mathbb{P}_Z]$ is reduced to zero, which results in the coincidence between \mathbb{P}_Z and $\widehat{\mathbb{P}}_Z$, indicating all predictive cues with view-consistency are preserved by the representation, and we have:

$$\lim_{D_{KL}[\widehat{\mathbb{P}}_Z || \mathbb{P}_Z] \rightarrow 0} I(y; z_i | z_{\{1,\dots,n\}/i}) = 0 \quad (41)$$

Based on Eq. (26), we show:

$$\lim_{D_{KL}[\widehat{\mathbb{P}}_Z || \mathbb{P}_Z] \rightarrow 0} I(y; z_i) - I_i^c = 0, \quad (42)$$

demonstrating that minimizing $D_{KL}[\mathbb{P}_{z_{\{1,\dots,n\}}} || \mathbb{P}_{z_{\{1,\dots,n\}/i}}]$ is consistent with the objective of eliminating view-specific information. Based on the above analysis, (T_1) is proved.

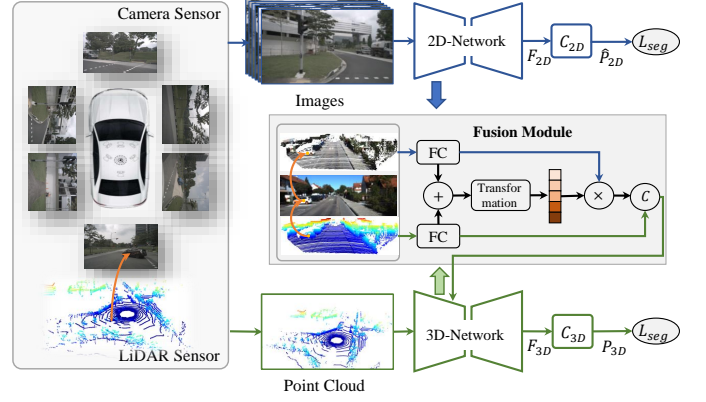


Fig. 12: Graphical illustration of the framework adopted in LiDAR-RGB semantic segmentation.

A.2 Proof to Thesis 2

As analyzed in A.1, MV^2D preserves all compositions included by I_i^c through Eq. (29). More specifically, as illustrated in Fig. 2, MV^2D would preserve $I_{y z_1 z_2 | z_3}$, $I_{y z_1 z_3 | z_2}$ and $I_{y z_1 z_2 z_3}$ for z_1 , and perform the same processes for the remaining ones, *i.e.*, z_2 , and z_3 . As a result, the learned representations $\{z_1, z_2, z_3\}$ encode $I_{y z_1 z_2 z_3}$ with a larger weight since it is shared by every viewpoint. Correspondingly, other components (*e.g.*, $I_{y z_1 z_2 | z_3}$, $I_{y z_1 z_3 | z_2}$) are assigned with smaller weights due to the partial sharing. On this basis, the preserved information would be automatically prioritized by MV^2D , which proves (T_2) .

APPENDIX B FRAMEWORK DETAILS

B.1 Cross-Modal Person Re-identification

To further investigate the effectiveness of the proposed MV^2D in 3-view circumstance, we adopt another viewpoint in addition to the default infrared and visible ones. More specifically, we deploy the U-Net [74] trained with Eq. (43) to obtain the additional viewpoint.

$$\mathcal{L}_{recon} = \omega \cdot \ell_2(x, x') + \text{Lap}_1(x, x'). \quad (43)$$

Note $\ell_2(x, x') = \|x - x'\|_2^2$ is the squared-loss function, and $\text{Lap}_1(x, x')$ denotes the Laplacian pyramid loss [75] defined as:

$$\text{Lap}_1(x, x') = \sum_j 2^{2j} |L^j(x) - L^j(x')|_1, \quad (44)$$

where $L^j(x)$ is the j -th level of the Laplacian pyramid representation of x .

B.2 LiDAR-RGB Semantic Segmentation

In this section, we elaborate the framework adopted in LiDAR-RGB semantic segmentation. As is shown in Fig. 12, we deploy two branches to handle inputs from both RGB and LiDAR sensors, and each of which is composed of one backbone network and one information bottleneck architecture to enable the use of VCD. Specifically, the 2-D network and 3-D network are implemented with SwiftNet [71] and SPVCNN [60], respectively. Besides, we also adopt a fusion module [70] which applies various transformation

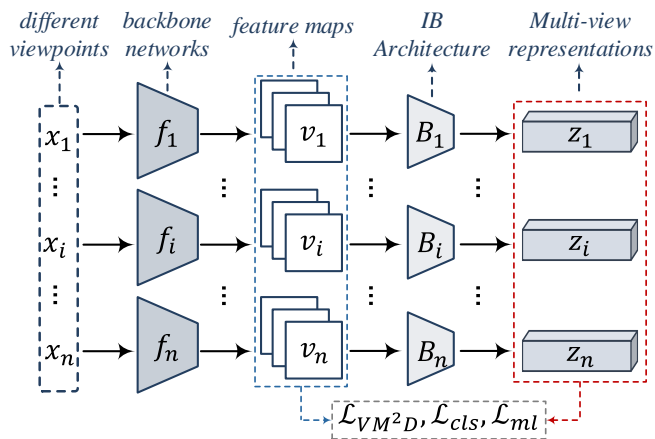


Fig. 13: Overall framework utilized for multi-view classification, where the subscriptions index different viewpoint.

(e.g., element-wise addition/product, concatenation) to the inputs of image and point cloud. The fused outputs are then utilized to facilitate 3-D representation learning. Note the segmentation loss \mathcal{L}_{seg} consists of multi-class focal loss [72], Lovász-softmax loss [73] and our VCD for better performance.

B.3 Multi-View Classification

In this section, we show more details of the adopted framework for multi-view classification. As is illustrated in Fig. 13, $\{f_i\}_{i=1}^n$ is a set of backbone networks utilized to transform the input to feature maps, which are then encoded into a series of multi-view representation with much lower dimensions. Note both $\{v_i\}_{i=1}^n$ and $\{z_i\}_{i=1}^n$ are entailed for loss computation, with \mathcal{L}_{MV^2D} , \mathcal{L}_{cls} and \mathcal{L}_{ml} denoted as the proposed multi-view variational distillation, cross-entropy and metric learning.

REFERENCES

- [1] G. Andrew, R. Arora, J. Bilmes, and K. Livescu, "Deep canonical correlation analysis," in *Proceedings of the International Conference on Machine Learning*, 2013, pp. 1247–1255.
- [2] W. Wang, R. Arora, K. Livescu, and J. Bilmes, "On deep multi-view representation learning," in *Proceedings of the International Conference on Machine Learning*, 2015, pp. 1083–1092.
- [3] M. Kan, S. Shan, H. Zhang, S. Lao, and X. Chen, "Multi-view discriminant analysis," *IEEE Transactions on Pattern Analysis and Machine Intelligence*, vol. 38, no. 1, pp. 188–194, 2015.
- [4] N. Tishby, F. C. Pereira, and W. Bialek, "The information bottleneck method," in *Proceedings of the Allerton Conference on Communication, Control and Computing*, 1999, pp. 368–377.
- [5] M. Federici, A. Dutta, P. Forré, N. Kushman, and Z. Akata, "Learning robust representations via multi-view information bottleneck," in *Proceedings of the International Conference on Learning Representations*, 2020.
- [6] C. Xu, D. Tao, and C. Xu, "Large-margin multi-view information bottleneck," *IEEE Transactions on Pattern Analysis and Machine Intelligence*, vol. 36, no. 8, pp. 1559–1572, 2014.
- [7] Z. Wan, C. Zhang, P. Zhu, and Q. Hu, "Multi-view information-bottleneck representation learning," in *Proceedings of the AAAI Conference on Artificial Intelligence*, 2021, pp. 10 085–10 092.
- [8] R. D. Hjelm, A. Fedorov, S. Lavoie-Marchildon, K. Grewal, P. Bachman, A. Trischler, and Y. Bengio, "Learning deep representations by mutual information estimation and maximization," in *Proceedings of the International Conference on Learning Representations*, 2019.
- [9] B. Poole, S. Ozair, A. Van Den Oord, A. Alemi, and G. Tucker, "On variational bounds of mutual information," in *Proceedings of the International Conference on Machine Learning*, 2019, pp. 5171–5180.
- [10] M. I. Belghazi, A. Baratin, S. Rajeshwar, S. Ozair, Y. Bengio, A. Courville, and D. Hjelm, "Mutual information neural estimation," in *Proceedings of the International Conference on Machine Learning*, 2018, pp. 531–540.
- [11] A. A. Alemi, I. Fischer, J. V. Dillon, and K. Murphy, "Deep variational information bottleneck," in *Proceedings of the International Conference on Learning Representations*, 2017.
- [12] Z. Piran, R. Shwartz-Ziv, and N. Tishby, "The dual information bottleneck," *CoRR*, vol. abs/2006.04641, 2020.
- [13] X. Tian, Z. Zhang, S. Lin, Y. Qu, Y. Xie, and L. Ma, "Farewell to mutual information: Variational distillation for cross-modal person re-identification," in *Proceedings of the IEEE/CVF Conference on Computer Vision and Pattern Recognition*, 2021, pp. 1522–1531.
- [14] N. Tishby and N. Zaslavsky, "Deep learning and the information bottleneck principle," in *IEEE Information Theory Workshop*, 2015, pp. 1–5.
- [15] D. Felice and N. Ay, "Divergence functions in information geometry," in *Proceedings of the International Conference on Geometric Science of Information*, 2019, pp. 433–442.
- [16] X. B. Peng, A. Kanazawa, S. Toyer, P. Abbeel, and S. Levine, "Variational discriminator bottleneck: Improving imitation learning, inverse rl, and gans by constraining information flow," in *Proceedings of the International Conference on Learning Representations*, 2019.
- [17] R. K. Mahabadi, Y. Belinkov, and J. Henderson, "Variational information bottleneck for effective low-resource fine-tuning," in *Proceedings of the International Conference on Learning Representations*, 2021.
- [18] K. Schulz, L. Sixt, F. Tombari, and T. Landgraf, "Restricting the flow: Information bottlenecks for attribution," in *Proceedings of the International Conference on Learning Representations*, 2020.
- [19] S. Ma, D. McDuff, and Y. Song, "Unpaired image-to-speech synthesis with multimodal information bottleneck," in *Proceedings of the IEEE/CVF International Conference on Computer Vision*, 2019, pp. 7598–7607.
- [20] S. Sinha, H. Bharadhwaj, A. Goyal, H. Larochelle, A. Garg, and F. Shkurti, "DIBS: diversity inducing information bottleneck in model ensembles," in *Proceedings of the AAAI Conference on Artificial Intelligence*, 2021, pp. 9666–9674.
- [21] E. Schneidman, N. Slonim, N. Tishby, R. R. van Steveninck, and W. Bialek, "Analyzing neural codes using the information bottleneck method," in *Proceedings of the Advances in Neural Information Processing Systems*, 2001.
- [22] S. Bang, P. Xie, H. Lee, W. Wu, and E. Xing, "Explaining a black-box by using a deep variational information bottleneck approach," in *Proceedings of the AAAI Conference on Artificial Intelligence*, 2021, pp. 11 396–11 404.
- [23] Y. Bengio, A. C. Courville, and P. Vincent, "Representation learning: A review and new perspectives," *IEEE Transactions on Pattern Analysis and Machine Intelligence*, vol. 35, no. 8, pp. 1798–1828, 2013.
- [24] T. Chen, S. Kornblith, M. Norouzi, and G. Hinton, "A simple framework for contrastive learning of visual representations," in *International Conference on Machine Learning*, 2020, pp. 1597–1607.
- [25] N. Chen, J. Zhu, F. Sun, and E. P. Xing, "Large-margin predictive latent subspace learning for multiview data analysis," *IEEE Transactions on Pattern Analysis and Machine Intelligence*, vol. 34, no. 12, pp. 2365–2378, 2012.
- [26] H. Park, S. Lee, J. Lee, and B. Ham, "Learning by aligning: Visible-infrared person re-identification using cross-modal correspondences," in *Proceedings of the IEEE/CVF International Conference on Computer Vision*, 2021, pp. 12 046–12 055.
- [27] M. Kan, S. Shan, H. Zhang, S. Lao, and X. Chen, "Multi-view discriminant analysis," *IEEE Transactions on Pattern Analysis and Machine Intelligence*, vol. 38, no. 1, pp. 188–194, 2015.
- [28] J. Xu, W. Li, X. Liu, D. Zhang, J. Liu, and J. Han, "Deep embedded complementary and interactive information for multi-view classification," in *Proceedings of the AAAI Conference on Artificial Intelligence*, 2020, pp. 6494–6501.
- [29] Y. Li, M. Yang, and Z. Zhang, "A survey of multi-view representation learning," *IEEE Transactions on Knowledge and Data Engineering*, vol. 31, no. 10, pp. 1863–1883, 2019.
- [30] C. Xu, D. Tao, and C. Xu, "A survey on multi-view learning," *arXiv preprint arXiv:1304.5634*, 2013.
- [31] S. I. Mirzadeh, M. Farajtabar, A. Li, N. Levine, A. Matsukawa, and H. Ghasemzadeh, "Improved knowledge distillation via teacher

- assistant," in *Proceedings of the AAAI Conference on Artificial Intelligence*, 2020, pp. 5191–5198.
- [32] Y. Zhang, T. Xiang, T. M. Hospedales, and H. Lu, "Deep mutual learning," in *Proceedings of the IEEE/CVF Conference on Computer Vision and Pattern Recognition*, 2018, pp. 4320–4328.
- [33] L. Zhang, J. Song, A. Gao, J. Chen, C. Bao, and K. Ma, "Be your own teacher: Improve the performance of convolutional neural networks via self distillation," in *Proceedings of the IEEE/CVF International Conference on Computer Vision*, 2019, pp. 3713–3722.
- [34] J. Gou, B. Yu, S. J. Maybank, and D. Tao, "Knowledge distillation: A survey," *Int. J. Comput. Vis.*, vol. 129, no. 6, pp. 1789–1819, 2021.
- [35] A. Achille and S. Soatto, "Emergence of invariance and disentanglement in deep representations," *The Journal of Machine Learning Research*, vol. 19, no. 1, pp. 1947–1980, 2018.
- [36] H. Hwang, G. Kim, S. Hong, and K. Kim, "Variational interaction information maximization for cross-domain disentanglement," in *Proceedings of the Advances in Neural Information Processing Systems*, 2020, pp. 22 479–22 491.
- [37] X. Sun, Y. Xu, P. Cao, Y. Kong, L. Hu, S. Zhang, and Y. Wang, "Tcgm: An information-theoretic framework for semi-supervised multi-modality learning," in *Proceedings of the European Conference on Computer Vision*, 2020, pp. 171–188.
- [38] H. Hwang, G. Kim, S. Hong, and K. Kim, "Variational interaction information maximization for cross-domain disentanglement," in *Proceedings of the Advances in Neural Information Processing Systems*, 2020, pp. 22 479–22 491.
- [39] S. Choi, S. Lee, Y. Kim, T. Kim, and C. Kim, "Hi-cmd: Hierarchical cross-modality disentanglement for visible-infrared person re-identification," in *Proceedings of the IEEE/CVF Conference on Computer Vision and Pattern Recognition*, 2020, pp. 10 257–10 266.
- [40] M. Ye, J. Shen, D. J. Crandall, L. Shao, and J. Luo, "Dynamic dual-attentive aggregation learning for visible-infrared person re-identification," in *Proceedings of the European Conference on Computer Vision*, 2020, pp. 229–247.
- [41] Y. Chen, L. Wan, Z. Li, Q. Jing, and Z. Sun, "Neural feature search for rgb-infrared person re-identification," in *Proceedings of the IEEE/CVF Conference on Computer Vision and Pattern Recognition*, 2021, pp. 587–597.
- [42] X. Hao, S. Zhao, M. Ye, and J. Shen, "Cross-modality person re-identification via modality confusion and center aggregation," in *Proceedings of the IEEE/CVF International Conference on Computer Vision*, 2021, pp. 16 403–16 412.
- [43] Z. Wei, X. Yang, N. Wang, and X. Gao, "Syncretic modality collaborative learning for visible infrared person re-identification," in *Proceedings of the IEEE/CVF International Conference on Computer Vision*, 2021, pp. 225–234.
- [44] C. Fu, Y. Hu, X. Wu, H. Shi, T. Mei, and R. He, "Cm-nas: Cross-modality neural architecture search for visible-infrared person re-identification," in *Proceedings of the IEEE/CVF International Conference on Computer Vision*, 2021, pp. 11 823–11 832.
- [45] M. Ye, J. Shen, G. Lin, T. Xiang, L. Shao, and S. C. Hoi, "Deep learning for person re-identification: A survey and outlook," *IEEE Transactions on Pattern Analysis and Machine Intelligence*, 2021.
- [46] A. Wu, W.-S. Zheng, H.-X. Yu, S. Gong, and J. Lai, "Rgb-infrared cross-modality person re-identification," in *Proceedings of the IEEE/CVF International Conference on Computer Vision*, 2017, pp. 5380–5389.
- [47] D. T. Nguyen, H. G. Hong, K. W. Kim, and K. R. Park, "Person recognition system based on a combination of body images from visible light and thermal cameras," *Sensors*, vol. 17, no. 3, p. 605, 2017.
- [48] X. Wang, Y. Hua, E. Kodirov, G. Hu, R. Garnier, and N. M. Robertson, "Ranked list loss for deep metric learning," in *Proceedings of the IEEE/CVF Conference on Computer Vision and Pattern Recognition*, 2019, pp. 5207–5216.
- [49] L. Fei-Fei, R. Fergus, and P. Perona, "Learning generative visual models from few training examples: An incremental bayesian approach tested on 101 object categories," *Computer Vision and Image Understanding*, vol. 106, no. 1, pp. 59–70, 2007.
- [50] Y. Li, F. Nie, H. Huang, and J. Huang, "Large-scale multi-view spectral clustering via bipartite graph," in *Proceedings of the AAAI Conference on Artificial Intelligence*, 2015, pp. 2750–2756.
- [51] C. H. Lampert, H. Nickisch, and S. Harmeling, "Learning to detect unseen object classes by between-class attribute transfer," in *Proceedings of the IEEE/CVF International Conference on Computer Vision*, 2009, pp. 951–958.
- [52] T.-S. Chua, J. Tang, R. Hong, H. Li, Z. Luo, and Y. Zheng, "Nus-wide: a real-world web image database from national university of singapore," in *Proceedings of the ACM International Conference on Image and Video Retrieval*, 2009, pp. 1–9.
- [53] M. Amini, N. Usunier, and C. Goutte, "Learning from multiple partially observed views - an application to multilingual text categorization," in *Proceedings of the Advances in Neural Information Processing Systems*, 2009, pp. 28–36.
- [54] D. Dua and C. Graff, "UCI machine learning repository," 2017.
- [55] J. Cheng and P. Baldi, "Improved residue contact prediction using support vector machines and a large feature set," *BMC bioinformatics*, vol. 8, no. 1, pp. 1–9, 2007.
- [56] M. Dorfer, R. Kelz, and G. Widmer, "Deep linear discriminant analysis," in *Proceedings of the International Conference on Learning Representations*, 2016.
- [57] V. Uurtio, S. Bhadra, and J. Rousu, "Large-scale sparse kernel canonical correlation analysis," in *Proceedings of the International Conference on Machine Learning*, 2019, pp. 6383–6391.
- [58] C. Zhang, Y. Cui, Z. Han, J. T. Zhou, H. Fu, and Q. Hu, "Deep partial multi-view learning," *IEEE Transactions on Pattern Analysis and Machine Intelligence*, vol. 44, no. 5, pp. 2402–2415, 2022.
- [59] A. Milioto, I. Vizzo, J. Behley, and C. Stachniss, "Rangenet++: Fast and accurate lidar semantic segmentation," in *Proceedings of the International Conference on Intelligent Robots and Systems*, 2019, pp. 4213–4220.
- [60] H. Tang, Z. Liu, S. Zhao, Y. Lin, J. Lin, H. Wang, and S. Han, "Searching efficient 3d architectures with sparse point-voxel convolution," in *Proceedings of the European Conference on Computer Vision*, 2020, pp. 685–702.
- [61] Y. Zhang, Z. Zhou, P. David, X. Yue, Z. Xi, B. Gong, and H. Foroosh, "Polarnet: An improved grid representation for online lidar point clouds semantic segmentation," in *Proceedings of the IEEE/CVF Conference on Computer Vision and Pattern Recognition*, 2020, pp. 9601–9610.
- [62] X. Zhu, H. Zhou, T. Wang, F. Hong, Y. Ma, W. Li, H. Li, and D. Lin, "Cylindrical and asymmetrical 3d convolution networks for lidar segmentation," in *Proceedings of the IEEE/CVF Conference on Computer Vision and Pattern Recognition*, 2021, pp. 9939–9948.
- [63] R. Cheng, R. Razani, E. Taghavi, E. Li, and B. Liu, "2-s3net: Attentive feature fusion with adaptive feature selection for sparse semantic segmentation network," in *Proceedings of the IEEE/CVF Conference on Computer Vision and Pattern Recognition*, 2021, pp. 12 547–12 556.
- [64] Z. Zhuang, R. Li, K. Jia, Q. Wang, Y. Li, and M. Tan, "Perception-aware multi-sensor fusion for 3d lidar semantic segmentation," in *Proceedings of the IEEE/CVF International Conference on Computer Vision*, 2021, pp. 16 280–16 290.
- [65] Q. Hu, B. Yang, L. Xie, S. Rosa, Y. Guo, Z. Wang, N. Trigoni, and A. Markham, "Randla-net: Efficient semantic segmentation of large-scale point clouds," in *Proceedings of the IEEE/CVF Conference on Computer Vision and Pattern Recognition*, 2020, pp. 11 108–11 117.
- [66] S. Qiu, S. Anwar, and N. Barnes, "Semantic segmentation for real point cloud scenes via bilateral augmentation and adaptive fusion," in *Proceedings of the IEEE/CVF Conference on Computer Vision and Pattern Recognition*, 2021, pp. 1757–1767.
- [67] X. Yan, J. Gao, J. Li, R. Zhang, Z. Li, R. Huang, and S. Cui, "Sparse single sweep lidar point cloud segmentation via learning contextual shape priors from scene completion," in *Proceedings of the AAAI Conference on Artificial Intelligence*, 2021, pp. 3101–3109.
- [68] H. Caesar, V. Bankiti, A. H. Lang, S. Vora, V. E. Liong, Q. Xu, A. Krishnan, Y. Pan, G. Baldan, and O. Beijbom, "nuscenes: A multimodal dataset for autonomous driving," in *Proceedings of the IEEE/CVF conference on Computer Vision and Pattern Recognition*, 2020, pp. 11 621–11 631.
- [69] J. Behley, M. Garbade, A. Milioto, J. Quenzel, S. Behnke, C. Stachniss, and J. Gall, "Semantickitti: A dataset for semantic scene understanding of lidar sequences," in *Proceedings of the IEEE/CVF International Conference on Computer Vision*, 2019, pp. 9297–9307.
- [70] T. Huang, Z. Liu, X. Chen, and X. Bai, "Epnnet: Enhancing point features with image semantics for 3d object detection," in *Proceedings of the European Conference on Computer Vision*, 2020, pp. 35–52.
- [71] H. Wang, X. Jiang, H. Ren, Y. Hu, and S. Bai, "Swiftnet: Real-time video object segmentation," in *Proceedings of the IEEE/CVF Conference on Computer Vision and Pattern Recognition*, 2021, pp. 1296–1305.
- [72] T.-Y. Lin, P. Goyal, R. Girshick, K. He, and P. Dollár, "Focal loss for

- dense object detection," in *Proceedings of the IEEE/CVF International Conference on Computer Vision*, 2017, pp. 2980–2988.
- [73] M. Berman, A. R. Triki, and M. B. Blaschko, "The lovász-softmax loss: A tractable surrogate for the optimization of the intersection-over-union measure in neural networks," in *Proceedings of the IEEE/CVF Conference on Computer Vision and Pattern Recognition*, 2018, pp. 4413–4421.
- [74] O. Ronneberger, P. Fischer, and T. Brox, "U-net: Convolutional networks for biomedical image segmentation," in *International Conference on Medical image computing and computer-assisted intervention*, 2015, pp. 234–241.
- [75] W.-S. Lai, J.-B. Huang, N. Ahuja, and M.-H. Yang, "Deep laplacian pyramid networks for fast and accurate super-resolution," in *Proceedings of the IEEE/CVF Conference on Computer Vision and Pattern Recognition*, 2017, pp. 624–632.